Accurate mapping of spherically symmetric black holes in a parametrized framework

Prashant Kocherlakota[1,*] and Luciano Rezzolla[1,2]

[1]*Institut für Theoretische Physik, Goethe-Universität, Max-von-Laue-Straße 1, 60438 Frankfurt, Germany*
[2]*School of Mathematics, Trinity College, Dublin 2, Ireland*

(Received 30 July 2020; accepted 28 August 2020; published 23 September 2020)

The Rezzolla-Zhidenko (RZ) framework provides an efficient approach to characterize spherically symmetric black hole spacetimes in arbitrary metric theories of gravity using a small number of variables [Rezzolla and Zhidenko, Phys. Rev. D **90**, 084009 (2014)]. These variables can be obtained in principle from near-horizon measurements of various astrophysical processes, thus potentially enabling efficient tests of both black hole properties and the theory of general relativity in the strong-field regime. Here, we extend this framework to allow for the parametrization of arbitrary asymptotically flat, spherically symmetric metrics and introduce the notion of an 11-dimensional (11D) parametrization space Π, on which each solution can be visualized as a curve or surface. An $\mathcal{L}^2$ norm on this space is used to measure the deviation of a particular compact object solution from the Schwarzschild black hole solution. We calculate various observables, related to particle and photon orbits, within this framework and demonstrate that the relative errors we obtain are low (about 10^{-6}). In particular, we obtain the innermost stable circular orbit (ISCO) frequency, the unstable photon-orbit impact parameter (shadow radius), the entire orbital angular speed profile for circular Kepler observers, and the entire lensing deflection angle curve for various types of compact objects, including nonsingular and singular black holes, boson stars, and naked singularities, from various theories of gravity. Finally, we provide in a tabular form the first 11 coefficients of the fourth-order RZ parametrization needed to describe a variety of commonly used black hole spacetimes. When comparing with the first-order RZ parametrization of astrophysical observables such as the ISCO frequency, the coefficients provided here increase the accuracy by 2 orders of magnitude or more.

DOI: 10.1103/PhysRevD.102.064058

I. INTRODUCTION

The Dicke-Eötvös experiment established that the trajectories of freely falling test bodies are independent of their internal structures and compositions, thereby setting the weak equivalence principle (WEP) on firm footing. Truly remarkable tests of whether the speed of light is isotropic and independent of the velocity of the source, and tests of time dilation, conservation of four-momentum, and the relativistic laws of kinematics in particle physics experiments have all bolstered our confidence in the principles of local Lorentz invariance (LLI) and local positional invariance (LPI) as being fundamental features of any serious physical theory. Therefore, the Einstein equivalence principle (EEP), which requires LLI, LPI, and WEP all to hold, is well supported by experiments to date. For further details, we direct the reader to see the foundational papers in experimental gravitation [1,2], and an excellent modern review can be found in Ref. [3].

Assuming the exact validity of the EEP implies that metric theories of gravity are the most viable candidates to describe classical gravity, or possibly theories that are metric apart from very weak or short-range nonmetric couplings (as in string theory) [1–3]. Following Ref. [1], we define a metric theory as one in which a metric tensor $\boldsymbol{g}$ exists and is necessarily associated with gravity, while matter and other nongravitational fields obey $\nabla \cdot \boldsymbol{T} = 0$, where ∇ is defined with respect to the metric $\boldsymbol{g}$, and $\boldsymbol{T}$ is the energy-momentum-stress tensor for all matter and nongravitational fields [1]. The latter condition on $\boldsymbol{T}$ has the important consequence that test bodies move on geodesics of $\boldsymbol{g}$, which is of central importance here [4]. Gravitational redshift, bending of light due to spacetime curvature, frame-dragging effects due to matter currents, and the Shapiro delay are to be expected in any metric theory of gravity, and one can test candidate theories quantitatively, in the weak-field limit, for their agreement with such observables within the parametrized post-Newtonian (PPN) parametrization scheme proposed in Refs. [5,6], in terms of ten variables.

General relativity (GR; see Ref. [7]), which is the Occam's razor theory of gravity, has withstood all classical weak-field tests to date successfully [3,8], and an early success of GR in the strong-field regime was the prediction of the rate of energy loss due to gravitational wave radiation

*kocherlakota@itp.uni-frankfurt.de

in binary pulsar systems [9]. More recently, with major large-scale astronomy missions such as the Laser Interferometric Gravitational wave Observatory (LIGO) and the Event Horizon Telescope (EHT; Refs. [10–15]), it is becoming possible to observe astrophysical events that are dominated by strong-gravity effects. Direct detections of gravitational waves by LIGO from various compact binary systems [16,17] and the recently obtained image of the supermassive compact object M87⋆ by EHT [10–15] can be interpreted consistently with the use of the black hole (BH) solutions of GR. The recent observations by GRAVITY of the gravitational redshift [18] and geodetic orbit precession [19] of the star S2 near our Galaxy's central supermassive compact object Sgr A⋆ are other key successes of GR in strong gravitational fields.

Various non-BH solutions, such as boson stars and naked singularities, also exhibit many of the features that BH solutions do, such as the presence of photon spheres [20,21], and characterizing observable differences of such "mimickers" from the BHs of GR is clearly important. Attempting to address the question of the validity of the cosmic censorship hypothesis from an observational point of view is an attractive possibility: while general results like the Birkhoff theorem [22], along with various other analytical [23–31] and numerical studies [32–36], lend weight to our expectation that BHs can, in fact, occur frequently—or equivalently, that they do form generically as end states of continual gravitational collapse—despite significant effort [37–44], we have not been able to rule out the formation of naked singularities in GR.

Of course, the very presence of spacetime singularities, which are locations of arbitrarily large curvature, in the various solutions of GR is a long-standing weakness of the theory. Their existence is assuredly generic [45–48], and their formation is independent of whether or not they are sheathed behind event horizons (see, e.g., Refs. [49,50]). Therefore, it is useful to study observables associated with regular solutions for BH-like compact objects, both within GR and in alternative theories of gravity, to check whether they are consistent with recent strong-gravity measurements of, e.g., the M87⋆ shadow size recently obtained by the EHT, and to explore whether they are better models for compact astrophysical objects.

Since the number of models for compact objects offered by various candidate theories of gravity (sometimes when coupled to other fields) is large, when attempting to test the theory of general relativity using strong-field observables, it is imperative that we have a unified-theory-agnostic framework ready that characterizes arbitrary solutions (BHs and non-BHs) efficiently—i.e., with as few parameters as possible. Toward this end, we extend here the framework presented in Ref. [51], which can be used to test properties of asymptotically flat, spherically symmetric BH solutions from arbitrary metric theories of gravity, to include non-BH solutions as well. Our parametrization framework uses 11 parameters, and we are able to obtain approximate values for the metrics and various observables for a variety of compact objects at typical relative errors of 10^{-6}. The observables we choose to study here are the orbital angular speeds of test bodies moving on circular geodesics, the impact parameter of photons on unstable circular geodesics (shadow radius), and the angle of deflection due to gravitational lensing; a study of these observables is important when considering the construction of images of compact objects from general-relativistic magnetohydrodynamic (GRMHD) simulations. We also report here the deviations of these observables from their corresponding values for the Schwarzschild BH for easy comparison.

Finally, since EEP may only hold approximately—i.e., since it could be violated in the strong-field regime (see, e.g., Refs. [52,53])—it is imperative that the framework we use here to set up strong-field tests of theories of gravity be able to characterize BH solutions from theories that break: e.g., LLI (as in Einstein-aether theories [54]) or even nonmetric theories in which, e.g., the electromagnetic Lagrangian is modified to allow for nonlinear interactions [55]. Therefore, the models for compact objects we consider here are BHs from (a) GR (that are either singular [56,57] or nonsingular [58–61]), (b) Einstein-aether theory [62], (c) string theory [63–67], and (d) GR coupled to nonlinear electrodynamics [68,69]. Additionally, we also consider spacetimes of regular mini–boson stars [21] and naked singularities [70] in GR. We argue that since the level of errors in approximating their exact observables is sufficiently low, it is possible to distinguish between these objects extremely well whenever their exact variables differ within the present framework.

The outline of the paper is as follows: In Sec. II, we discuss a unified framework to parametrize and implement strong- and weak-field tests of arbitrary spherically symmetric metrics in arbitrary metric theories of gravity (and some that are nonmetric, as mentioned above). We note that this is a smooth extension of the Rezzolla-Zhidenko parametrization scheme presented in Ref. [51]. In Sec. III, we outline how various observables related to causal geodesics may be computed within this parametrization scheme. In Sec. IV, we introduce the notion of an 11D parametrization space Π on which every metric solution can be uniquely visualized, and provide brief descriptions of the various compact objects under consideration here. We also demonstrate the efficiency of our framework in obtaining the metric functions (up to two derivatives) across the entire region of interest. For example, for BHs, we are able to approximate their entire exterior geometry to a maximum relative error that is typically less than 10^{-6}. We also show how all of the associated observables considered here are recovered at similar error levels. Section V presents a summary of our results and discusses various advantages of this framework. Our results have considerable overlap with the analysis for BHs presented in Ref. [71], and we briefly compare the two sets of results in Sec. V.

II. AN EFFICIENT PARAMETRIZATION FRAMEWORK FOR SPHERICALLY SYMMETRIC SPACETIMES

The Rezzolla-Zhidenko (RZ) framework of parametrizing asymptotically flat, spherically symmetric BH spacetimes in arbitrary metric theories of gravity [51] effectively rewrites a portion of the metric functions in terms of continued fractions over a conformal radial coordinate. A smooth extension of this scheme was proposed in Ref. [72] to tackle the problem of parametrizing the broader class of asymptotically flat, axially symmetric BH spacetimes, when the metric is expressed in Boyer-Lindquist-like coordinates (t, r, θ, ϕ). The existence of the two Killing vector fields ∂_t and ∂_ϕ ensures that the four free metric functions depend only on r and θ, and in the Konoplya-Rezzolla-Zhidenko (KRZ) framework [72], a double expansion in these variables is employed to parametrize them. In particular, a Taylor expansion in $y = \cos\theta$ and a mixed Taylor-Padé expansion in terms of a conformal radial coordinate x, similar to the one used here, efficiently parametrizes the exterior horizon geometry. We direct the reader toward Ref. [73] for a demonstration of the efficiency of the KRZ scheme in parametrizing various well-known stationary BH metrics and their associated shadow curves.

Restricting our focus to spherically symmetric spacetimes, we now discuss an extension of the RZ scheme that allows for arbitrary asymptotically flat, static spacetimes, including non-BH ones, to also be similarly characterized.

The line element outside a spherically symmetric configuration of matter can generally be expressed in arbitrary spherical-polar coordinates (t, ρ, θ, ϕ) as

$$ds^2 = -f(\rho)dt^2 + g(\rho)d\rho^2 + h(\rho)d\Omega_2^2, \tag{1}$$

where $d\Omega_2^2$ is the standard line element of a two-sphere. Since the aim of the current parametrization scheme is to compare metrics across arbitrary metric theories of gravity, it is useful to reexpress them in a standardized form, in the same set of "areal-radial, polar" coordinates (t, r, θ, ϕ), as

$$ds^2 = -N^2(r)dt^2 + \frac{B^2(r)}{N^2(r)}dr^2 + r^2d\Omega_2^2. \tag{2}$$

This radial coordinate r cleanly determines the proper area of two-spheres $\mathcal{A}$ in the spacetime as $\mathcal{A} = 4\pi r^2$. The desired coordinate transformation $\rho \to r$ to achieve this change in form can be obtained by solving for $\rho(r)$ from

$$h(\rho) = r^2, \tag{3}$$

with the other metric functions then being given as $N^2(r) = f(\rho(r))$ and $B^2(r) = f(\rho(r))g(\rho(r))(\partial_r\rho(r))^2$, where ∂_r represents a derivative with respect to r.

One can then compactify the radial coordinate by introducing an interior cutoff for it at $r = r_0 > 0$ and defining a conformal radial coordinate x as[1]

$$x(r) = 1 - \frac{r_0}{r}, \tag{4}$$

and the coordinate patch we will be interested in characterizing here is $r_0 \le r < \infty$. Clearly, $x(r = r_0) = 0$, and as $r \to \infty$, $x(r) \to 1$. Therefore, characterizing the metric functions $N^2(x)$ and $B^2(x)$ over the range $0 \le x < 1$ is equivalent to fully characterizing the spacetime over this radial range. It is useful to keep in mind the nature of this scale—i.e., a radial range $r_0 < r < 2r_0$ takes up almost half of the range of the conformal coordinate $0 < x < .5$. Also, the range $10^4 r_0 < r < 10^6 r_0$ is packed into $1\text{–}10^{-4} < x < 1\text{–}10^{-6}$.

When a metric [Eq. (2)] describes the geometry outside a BH, a natural choice for r_0 exists: namely, the location of its event horizon, since one is typically interested in studying features of its exterior geometry. Indeed, this will be our choice here.[2]

Similarly, if one is interested in studying the exterior geometry of a star, one can set r_0 to correspond to the location of its surface. In the case of a spacetime containing no such natural interior boundary, like that of a boson star or a naked singularity, one can set r_0 freely to a finite nonzero value. Since the central objective of the present study is to study differences of metric functions and observables associated with various compact objects from the Schwarzschild BH in particular, a convenient choice for r_0 here, for such objects, is $r_0 = 2M$, where M is the Arnowitt-Deser-Misner (ADM; Ref. [74]) mass of the spacetime. Since we will be considering asymptotically flat spacetimes exclusively here, identifying M is typically possible. This also reduces the number of requisite parameters from 12 to 11, as we will see below.

As noted above, a fundamental necessity to be able to constrain deviations from GR is a unified-theory-agnostic framework that characterizes both the strong and weak gravitational field regimes of arbitrary solutions efficiently. Since, by construction, the RZ parametrization scheme handles both these regimes simultaneously and effectively for spherically symmetric BH solutions [51], a natural choice is to extend it to include non-BH solutions. This is achieved by modifying the auxiliary function $A(x)$ used in Ref. [51] as

[1]Note that x is not a conformally *flat* coordinate. See the Appendix A for a discussion on how x is related to the conformally flat "tortoise" coordinate r_*.

[2]To be precise, when various types of horizons for a BH solution do not match (e.g., Einstein-aether BHs [62]), we will always choose r_0 to correspond to the outermost Killing horizon, which is the location of the outermost zero of the null expansion, and is given by the outermost root of g_{rr}^{-1}, i.e., $N^2(r_0) = 0$.

$$N^2(x) = n_0 + A(x)x, \tag{5}$$

where $n_0 = N^2(r = r_0)$. In particular, when the metric (1) describes a BH spacetime, we have $n_0 = 0$, and this definition for $A(x)$ reduces to the one used in Eq. (4) of Ref. [51]. We have essentially modified the "inner" boundary condition on the 1D box $0 \leq x < 1$ for the g_{tt}-metric function.

For the Killing vector ∂_t to remain timelike [$\boldsymbol{g}(\partial_t \cdot \partial_t) = g_{tt} < 0$] outside the outermost Killing horizon, clearly we require

$$0 < A(x), \quad \text{for } 0 < x < 1. \tag{6}$$

If a non-BH spacetime admits a Killing surface at some location (perhaps in aether theories), one must set r_0 to correspond to that location. The non-BH spacetimes considered here do not admit such Killing surfaces,[3] and we will set $r_0 = 2M$ for them in Sec. IV.

Equation (6) implies that a continued fraction approximation for $A(x)$ is already a salient possibility. However, to facilitate an easy comparison with the PPN form of the metric [3,5], we first write out the asymptotic Taylor expansions (to the first few orders) of the metric functions A and B, and introduce two new auxiliary functions $\tilde{A}$ and $\tilde{B}$ as

$$A(x) = 1 - n_0 - \epsilon(1-x) + (a_0 - \epsilon)(1-x)^2 + \tilde{A}(x)(1-x)^3, \tag{7}$$

$$B(x) = 1 + b_0(1-x) + \tilde{B}(x)(1-x)^2. \tag{8}$$

In the above, we have also introduced three new constants ϵ, a_0, and b_0, which, along with n_0, can be used to test whether the spacetime in question satisfies the PPN constraints that arise from weak-field tests of gravity, as we will see in Sec. III A. This redefinition [Eqs. (7) and (8)] of the auxiliary functions has the consequence that these tilded auxiliary functions, $\tilde{A}$ and $\tilde{B}$, do not influence the values of the PPN parameters of the spacetime.

Thus far, we have roughly performed Taylor expansions of the metric functions when rewritten in terms of x (a variable that behaves as $1/r$) about $x = 0$ in Eq. (5) and $x = 1$ in Eqs. (7) and (8). At the core of the efficiency of the current parametrization scheme is the choice to characterize $\tilde{A}$ and $\tilde{B}$ as Padé approximants in the form of continued fractions as

$$\tilde{A}(x) = \frac{a_1}{1 + \frac{a_2 x}{1 + \frac{a_3 x}{1 + \cdots}}}, \qquad \tilde{B}(x) = \frac{b_1}{1 + \frac{b_2 x}{1 + \frac{b_3 x}{1 + \cdots}}}. \tag{9}$$

Therefore, the set of PPN coefficients n_0, ϵ, a_0, and b_0, along with the Padé expansion coefficients, a_i and b_i ($i > 0$), completely characterize arbitrary spherically symmetric spacetimes in arbitrary metric theories of gravity.

By definition, these coefficients $[a_i (i > 0)]$ can be obtained by Taylor-expanding the continued fractions in Eq. (9), and matching the Padé expansion coefficients order by order with the Taylor-expansion coefficients for $\tilde{A}(x)$, which we write formally as

$$\tilde{A}(x) = \sum_{i=0}^{\infty} \tilde{a}_{i+1} x^i. \tag{10}$$

Below, we show the first few Padé coefficients of a function $\tilde{A}(x)$ in terms of its Taylor coefficients,

$$\begin{aligned}
a_1 &= \tilde{a}_1, \qquad a_2 = -\frac{\tilde{a}_2}{\tilde{a}_1}, \qquad a_3 = -\frac{(\tilde{a}_3\tilde{a}_1 - \tilde{a}_2^2)}{\tilde{a}_2\tilde{a}_1}, \\
a_4 &= -\frac{(\tilde{a}_4\tilde{a}_2 - \tilde{a}_3^2)\tilde{a}_1}{(\tilde{a}_3\tilde{a}_1 - \tilde{a}_2^2)\tilde{a}_2}, \\
a_5 &= -\frac{(\tilde{a}_5(\tilde{a}_3\tilde{a}_1 - \tilde{a}_2^2) - \tilde{a}_4^2\tilde{a}_1 + 2\tilde{a}_4\tilde{a}_3\tilde{a}_2 - \tilde{a}_3^3)\tilde{a}_2}{(\tilde{a}_4\tilde{a}_2 - \tilde{a}_3^2)(\tilde{a}_3\tilde{a}_1 - \tilde{a}_2^2)}, \\
a_6 &= -\frac{(\tilde{a}_6(\tilde{a}_4\tilde{a}_2 - \tilde{a}_3^2) - \tilde{a}_5^2\tilde{a}_2 + 2\tilde{a}_5\tilde{a}_4\tilde{a}_3 - \tilde{a}_4^3)(\tilde{a}_3\tilde{a}_1 - \tilde{a}_2^2)}{(\tilde{a}_5(\tilde{a}_3\tilde{a}_1 - \tilde{a}_2^2) - \tilde{a}_4^2\tilde{a}_1 + 2\tilde{a}_4\tilde{a}_3\tilde{a}_2 - \tilde{a}_3^3)(\tilde{a}_4\tilde{a}_2 - \tilde{a}_3^2)},
\end{aligned} \tag{11}$$

to demonstrate that the map between two sets of expansion coefficients for the same function is nonlinear. The reader may have observed that the dependence of either type of coefficient on the other of the same order is linear.

Henceforth, by an nth-order approximation, we will mean that we have truncated the Padé approximants by setting $a_{i>n} = 0$. The power of the present parametrization scheme is primarily due to the well-known property of the rapidity of the order-on-order convergence of Padé approximants [Eq. (9)] to the exact value for a multitude of functions [75,76], as compared to other approximation schemes, such as Taylor expansions [Eq. (10)], for example. That this well-known efficiency of Padé approximants is carried into the RZ parametrization has been demonstrated for the Einstein-dilaton spacetime [51], where the rate of convergence of order-on-order truncated Padé approximants was contrasted against the order-on-order truncated Taylor approximations of the Johannsen-Psaltis parametrization scheme in the Appendix of Ref. [51]. In Appendix B below, we conduct a similar convergence test against a recently proposed Taylor-expansion-based parametrization scheme [77] for the Bardeen-BH metric. See also Appendix C.

[3]The absence of a Killing horizon implies that stationary timelike Killing observers with four-velocities $u \propto \partial_t + \Omega\partial_\phi$ exist all the way to the center of the spacetime; these move on circular orbits. In the region where $N > r\partial_r N > 0$, equatorial circular geodesics ($\nabla_u u = 0$) exist [see Eq. (31) below]. For the non-BH spacetimes considered here, such equatorial Kepler observers can exist all the way to the center.

As we will see below in Sec. IV, already at the fourth order ($a_5 = b_5 = 0$), we are able to recover both metric functions for various spacetimes with a maximum relative error of about 10^{-6} over the entire range $0 \leq x < 1$, and not just close to the boundaries of the spacetime. In particular, for BH spacetimes, the relative errors are typically far lower at this order. In fact, it has recently been argued that already at the second order, one can recover the unstable photon-orbit radius, the orbital angular frequency of the innermost Kepler observer, and the quasinormal frequency spectrum for scalar perturbations to the desired accuracy for BH solutions that are not close to extremality [71].

For (metric) functions that are fractions of two polynomials, the associated continued fractions only have a finite (and typically small) number of coefficients a_i: i.e., for some n, all $a_{i>n} = 0$, and the nth-order Padé approximant converges exactly to the exact function (see, for example, the case of the Einstein-aether 1 BH in Sec. IV). However, as can be seen from the cases of the Bronnikov BH and the Janis-Newman-Winicour naked singularity below, even for nonpolynomial functions, the Padé approximant still converges fairly rapidly.

Note that it is not always possible to set a particular coefficient a_{n+1} to zero in order to obtain the nth-order truncated Padé approximant. One such instance is easily seen when $a_n < -1$: in this case, setting $a_{n+1} = 0$ creates a pole at $0 \leq x = -1/a_n < 1$ for the nth-order approximant. To get around such an obstacle, following the discussion in Sec. IV of Ref. [72], we may simply set $a_{n+2} = 0$, $a_{n+1} = 1$ and obtain then the approximation at the nth order.

It is now reasonable to ask how small a particular Padé coefficient a_n needs to be in order for higher-order coefficients to be neglected. One finds that such zeroes, $a_n \to 0$, are typically associated with poles at the next order, $a_{n+1} \to \pm\infty$, and it is clear that the combined effect of this zero-pole pair is to send $1 + a_n x/(1 + a_{n+1}x) \to 1$. Therefore, we argue that when $|a_n|$ is appropriately small, we can set $a_{i\geq n} = 0$.

We turn finally to the inner-boundary behavior of the metric functions in this parametrization scheme. The Taylor expansion of the metric functions near $x = 0$ is given as

$$N^2 = n_0 + (1 - n_0 - 2\epsilon + a_0 + a_1)x + (3\epsilon - 2a_0 - 3a_1 - a_1 a_2)x^2 + O(x^3), \tag{12}$$

$$\frac{B^2}{N^2} = \frac{n_0}{(1+b_0+b_1)^2} + \left(\frac{(1-n_0-2\epsilon+a_0+a_1)}{(1+b_0+b_1)^2} + \frac{2n_0(b_0+2b_1+b_1b_2)}{(1+b_0+b_1)^3}\right)x + O(x^2). \tag{13}$$

In the case of a BH spacetime ($n_0 = 0$), x measures the distance from the horizon, and therefore the above expressions capture the near-horizon geometry of a BH.

We end by noting that the condition given in Eq. (6) has the effect of setting nontrivial constraints on the allowed ranges of the expansion parameters ϵ, a_i for BH solutions—i.e., when working at a particular order n, the expansion parameters $\epsilon, a_{i\leq n}$ cannot be freely chosen. This is of considerable importance when employing this parametrization scheme to set up tests by solving inverse problems.

III. CHARACTERIZING OBSERVABLES IN THE PARAMETRIZATION SCHEME

In this section, we outline how various observables associated with spherically symmetric metrics can be obtained within the current parametrization scheme. In particular, we discuss how the PPN parameters, the orbital angular frequency of Kepler observers, and the deflection of light due to gravitational lensing can be calculated within this framework. We show also the calculation for the impact parameter of photons on unstable circular geodesics for completeness [51]. In addition to these observables, the method to obtain the quasinormal frequencies associated with scalar perturbations of spherically symmetric spacetimes within this parametrization scheme can also be found in Ref. [51]. We find it useful to note here that of the observables considered here, only the gravitational lensing deflection angle depends on the metric function B. When two spacetimes have identical N^2 functions, this observable can be used to distinguish between the two spacetimes (see, for example, the instances of the Hayward and modified Hayward BHs in Sec. IV).

A. Testing PPN constraints

The metric functions corresponding to a generic asymptotically flat spacetime can be expanded around asymptotic infinity, $x = 1$, and expressed as

$$N^2 = 1 - \frac{2M}{r_0}(1-x) + (\beta-\gamma)\frac{2M^2}{r_0^2}(1-x)^2 + O((1-x)^3),$$
$$\frac{B^2}{N^2} = 1 + \gamma\frac{2M}{r_0}(1-x) + O((1-x)^2), \tag{14}$$

where β and γ are parameters that can be obtained from the falloff features of the metric functions. For metric theories, β and γ are called parametrized post-Newtonian (PPN) parameters, and combinedly measure, e.g., the agreement of their predictions for the perihelion shift of Mercury and the time delay or light deflection due to the Sun; these satisfy [3]

$$|\beta - 1| \lesssim 2.3 \times 10^{-4}, \qquad |\gamma - 1| \lesssim 2.3 \times 10^{-5}. \tag{15}$$

The Taylor expansions of the metric functions around the exterior boundary of the spacetime can be obtained as

$$N^2 = 1 - (1 - n_0 + \epsilon)(1 - x) + a_0(1 - x)^2 + O((1 - x)^3),$$
$$\frac{B^2}{N^2} = 1 + (1 - n_0 + \epsilon + 2b_0)(1 - x) + O((1 - x)^2), \tag{16}$$

and upon comparing Eqs. (14) and (16), we can identify that

$$\epsilon = \frac{2M}{r_0} - (1 - n_0), \quad a_0 = \frac{2M^2}{r_0^2}(\beta - \gamma), \quad b_0 = \frac{M}{r_0}(\gamma - 1). \tag{17}$$

Therefore, the PPN constraints [Eq. (15)] then straightforwardly translate into constraints on the four constants introduced above (n_0, ϵ, a_0, and b_0) as

$$\mathcal{P}_1 = \left| \frac{2a_0}{(1 - n_0 + \epsilon)^2} + \frac{2b_0}{(1 - n_0 + \epsilon)} \right| \lesssim 2.3 \times 10^{-4},$$
$$\mathcal{P}_2 = \left| \frac{2b_0}{(1 - n_0 + \epsilon)} \right| \lesssim 2.3 \times 10^{-5}. \tag{18}$$

Note that a spacetime with vanishing zeroth-order parameters, a_0 and b_0, straightaway satisfies PPN constraints. Furthermore, it is also clear that the functions $\tilde{A}$ and $\tilde{B}$ do not contribute in any capacity toward asymptotic PPN constraints.

For non-BH spacetimes ($n_0 \neq 0$), if one sets $r_0 = 2M$, then $\epsilon = n_0$, and these constraints simplify to $\mathcal{P}_1 = |2a_0 + 2b_0|$ and $\mathcal{P}_2 = |2b_0|$, respectively. Notice that for BH spacetimes, since $n_0 = 0$, the parameter ϵ must satisfy $\epsilon > -1$ for the horizon to exist ($r_0 > 0$).

We also use the PPN constraints above [Eq. (18)] for all of the BH solutions coming from the nonmetric theories of gravity used here, since (a) for the dilaton BHs, despite the nonmetric coupling of the electrodynamics (ED) Lagrangian, photons still move along null geodesics of the metric [Eq. (2)][4]; and (b) for the nonlinear ED BHs, the Lagrangian reduces to Einstein-Hilbert-Maxwell in the weak-field limit [55,68,69]. We think it useful to mention here also that these BHs have the same asymptotic behavior as the BHs of GR (up to the relevant orders for PPN considerations). The Einstein-aether BHs considered here have $\beta = \gamma = 1$ (see, e.g., Refs. [79,80]). Note that we have made the rather strong assumption that even though these theories might not satisfy the Birkhoff theorem, these constraints are satisfied by astrophysical BHs.

[4]The dilaton gravity Lagrangian used here violates WEP in general due to a varying fine-structure constant (see, e.g., Ref. [78]), but not LLI or LPI.

B. Photon and particle orbits

Central to the comparison of images of compact objects that the EHT will obtain, such as Sgr A*, against GRMHD simulations is the study of the flow of matter in accretion disks near such objects, and of the motion of photons in the associated spacetime. As a first approximation, if the motion of accreting matter is modeled as being circularly freely falling, then a study of timelike stable circular geodesics becomes important. The radial infall speed of matter on such orbits is negligible compared to the speed at which it rotates around the compact object. In general, circular Kepler geodesics do not extend all the way into the black hole or up to the surface of a non-BH compact object, and there exists an innermost stable circular orbit (ISCO) at some radius $r = r_{\rm ISCO}$. Matter below this point, $r < r_{\rm ISCO}$, is pulled onto the compact object considerably more quickly. Therefore, local features of the flow of matter differ significantly depending on where the matter is relative to the ISCO, and the angular speed of matter at this location, $\Omega_{\rm ISCO}$, sets a dynamical free-fall timescale and constitutes an important observable of the compact object. Since this matter is typically a hot plasma, it emits radiation which is lensed by the gravity of the compact object before it reaches asymptotic observers present on Earth, for example. Some of these photons are also trapped by the compact object, depending on whether or not it possesses a photon sphere, which can be characterized by the impact parameter of the unstable circular photon orbit $\xi_{\rm ps}$. Essentially, (radially in-going) photons with impact parameter $\xi < \xi_{\rm ps}$ are captured by the central object and are on unstable orbits, as we will see below. Therefore, the union of the direction of all unstable null geodesics, from the point of view of an asymptotic observer, in a spacetime geometry, constitutes its shadow region, whose boundary is characterized by the photon sphere [81].

In this section, we will show how the Kepler orbital angular frequency profile $\Omega_{\rm K}(r)$, its ISCO value $\Omega_{\rm ISCO} \equiv \Omega_{\rm K}(r_{\rm ISCO})$, the light deflection angle due to gravitational lensing $\Delta\phi_{\rm GL}$, and the impact parameter of the photon on a circular unstable geodesic $\xi_{\rm ps}$ can be obtained within the present parametrization scheme. Toward this end, we begin with a brief discussion on circular causal geodesics, with a particular focus on unstable null and stable timelike ones. Since we are concerned with spherically symmetric spacetimes, a discussion of circular geodesics in the equatorial plane suffices [81].

The Lagrangian describing geodesic motion in a static spacetime [Eq. (1)] is given by

$$2\mathcal{L} = -N^2(r)\dot{t}^2 + \frac{B^2(r)}{N^2(r)}\dot{r}^2 + r^2\dot{\theta}^2 + r^2\sin^2\theta\dot{\phi}^2, \tag{19}$$

where the overdot represents a derivative with respect to the affine parameter. Since the Lagrangian is independent of t and ϕ, one obtains two constants of the motion, as

$$p_t \coloneqq \frac{\partial \mathcal{L}}{\partial \dot{t}} = -N^2\dot{t} = -E, \qquad p_\phi \coloneqq \frac{\partial \mathcal{L}}{\partial \dot{\phi}} = r^2\sin^2\theta\dot{\phi} = L, \tag{20}$$

where E and L are, respectively, the energy and angular momentum of the observer. We can rewrite Eq. (19) for geodesics restricted to the equatorial plane ($\theta = \pi/2$, $\dot{\theta} = 0$) as

$$\frac{B^2}{N^2}\dot{r}^2 + \left(\frac{L^2}{r^2} - \frac{E^2}{N^2} - 2\mathcal{L}\right) = 0, \tag{21}$$

where $2\mathcal{L} = 0$ for null geodesics and $2\mathcal{L} = -1$ for timelike geodesics. Let us define, for convenience, effective potentials for equatorial null (V) and timelike ($\tilde{V}$) observers as

$$V \coloneqq E^2\left(\frac{\xi^2}{r^2} - \frac{1}{N^2}\right), \tag{22}$$

$$\tilde{V} \coloneqq \tilde{E}^2\left(\frac{\tilde{\xi}^2}{r^2} - \frac{1}{N^2} + \frac{1}{\tilde{E}^2}\right), \tag{23}$$

where in the above we have introduced the impact parameter of a null observer as $\xi = L/E$, and analogously also the impact parameter $\tilde{\xi}$ of a timelike observer.

Equatorial circular null geodesics satisfy $\dot{r} = 0$ and $\ddot{r} = 0$, or equivalently $V = 0$ and $\partial_r V = 0$. The stability of a circular null geodesic is governed by the sign of $\partial_r^2 V$ ($-$ implies unstable). The expressions for the first and second derivatives of the effective potential are provided below for later use:

$$\frac{\partial_r V}{E^2} = -2\left(\frac{\xi^2}{r^3} - \frac{\partial_r N}{N^3}\right),$$
$$\frac{\partial_r^2 V}{E^2} = 6\left(\frac{\xi^2}{r^4} - \frac{(\partial_r N)^2}{N^4} + \frac{\partial_r^2 N}{3N^3}\right). \tag{24}$$

The stability of circular timelike geodesics can be similarly determined and the relevant expressions for $\partial_r\tilde{V}$ and $\partial_r^2\tilde{V}$ for them can be obtained simply by replacing all of the quantities in Eq. (24) with their tilded counterparts.

1. Photon sphere impact factor

As discussed above, equatorial circular null geodesics satisfy

$$0 = \frac{\xi^2}{r^2} - \frac{1}{N^2}, \qquad 0 = \frac{\xi^2}{r^3} - \frac{\partial_r N}{N^3}. \tag{25}$$

Equivalently, their radii $r = r_c$ can be found by solving

$$r - \frac{N(r)}{\partial_r N(r)} = 0. \tag{26}$$

If $\partial_r^2 V(r = r_c) < 0$, the spacetime has an unstable circular null geodesic at that location, and a stable circular null geodesic otherwise. Of these locations, that which corresponds to the absolute maximum of the null geodesic potential V marks the boundary of the shadow.[5]

We will denote this location by r_{ps}. The corresponding impact parameter ξ_{ps} of a photon on such an orbit is given as

$$\xi_{ps} = \frac{r_{ps}}{N(r_{ps})}. \tag{27}$$

While the photon sphere marks the boundary of the shadow region of a spacetime, when viewing the compact object from asymptotic infinity, due to gravitational lensing, we see it to be of size ξ_{ps} [81], which the EHT has observed. In terms of the conformal radial coordinate introduced above, $x = 1 - r_0/r$, we can now find the location of all allowed circular null geodesics by finding the solution $x = x_c$ of the equation [51]

$$(1 - x) - \frac{N(x)}{\partial_x N(x)} = 0, \tag{28}$$

where ∂_x denotes a derivative with respect to x. We denote by x_{ps} the location of the absolute maximum of the null geodesic potential, and the corresponding impact factor of this photon ξ_{ps} is given as

$$\xi_{ps} = \frac{r_0}{(1 - x_{ps})N(x_{ps})}. \tag{29}$$

2. Orbital angular velocity on stable circular geodesics

The class of equatorial Kepler observers in a static spacetime [Eq. (1)] correspond to stable circular timelike geodesic motion, and they satisfy, as discussed above,

$$0 = \frac{\tilde{\xi}^2}{r^2} - \frac{1}{N^2} + \frac{1}{\tilde{E}^2}, \qquad 0 = \frac{\tilde{\xi}^2}{r^3} - \frac{\partial_r N}{N^3}. \tag{30}$$

From the above, we can straightforwardly obtain the associated equatorial Kepler frequency at a given radius $\Omega_K = \dot{\phi}/\dot{t}$ as

$$\Omega_K \coloneqq \frac{\tilde{\xi}N^2}{r^2} = \sqrt{\frac{N(r)\partial_r N(r)}{r}}. \tag{31}$$

Furthermore, since around sufficiently massive black holes, pulsars (rotating neutron stars that spin around their axes

[5]It is to be noted that if there is no unstable circular null geodesic that corresponds to the location of the global maximum of the effective potential V, then such spacetimes do not cast shadows. Tangibly, one can imagine a spacetime that satisfies $\lim_{r\to 0} V(r) = \infty$, such as the Reissner-Nordström naked singularity spacetime, over a certain range of specific charge.

and emit radiation) can be treated as test objects and are visible to fixed asymptotic observers, measuring the rate at which pulses from them are recorded on Earth can be useful toward setting up strong-field tests of GR, since this rate depends on the properties of its motion. From pulse profiles of pulsars moving in the vicinity of static black holes, the orbital angular frequency can potentially be extracted, and since this frequency depends on the properties of the central compact object like the mass and charge of the central object, one could in principle extract these parameters for the spacetime as well [82].

A particle moving on the ISCO corresponds to the absolute minima of $\tilde{V}_{\rm eff}$, and it satisfies additionally $\partial_r^2 \tilde{V}_{\rm eff} = 0$, i.e.,

$$\frac{\tilde{\xi}^2}{r^4} - \frac{(\partial_r N)^2}{N^4} + \frac{\partial_r^2 N}{3N^3} = 0. \tag{32}$$

Clearly, the ISCO is also only marginally stable. The ISCO radius, then, is the solution of [51,83]

$$3N\partial_r N - 3r(\partial_r N)^2 + rN\partial_r^2 N = 0, \tag{33}$$

and the corresponding orbital angular velocity is given as $\Omega_{\rm ISCO} = \Omega_{\rm K}(r_{\rm ISCO})$. Kepler observers exist only outside the ISCO—i.e., only for $r \geq r_{\rm ISCO}$.

In the current parametrization scheme, the Kepler orbital angular velocity is given by

$$\Omega_{\rm K} = \frac{\sqrt{(1-x)^3 N(x)\partial_x N(x)}}{r_0}, \tag{34}$$

and the ISCO location is given as $r_{\rm ISCO} = r_0/(1 - x_{\rm ISCO})$, where $x_{\rm ISCO}$ satisfies

$$N\partial_x N - 3(1-x)(\partial_x N)^2 + (1-x)N\partial_x^2 N = 0. \tag{35}$$

Finally, the ISCO angular velocity is obtained from Eq. (34) by setting $x = x_{\rm ISCO}$.

3. Strong gravitational lensing

We study now the lensing properties of compact objects within this parametrization framework. For equatorial null geodesics, we can characterize the deflection due to gravity via

$$\begin{aligned}\frac{{\rm d}\phi}{{\rm d}r} = \frac{\dot{\phi}}{\dot{r}} &= \pm \frac{L/r^2}{(N/B)\sqrt{E^2/N^2 - L^2/r^2}} \\ &= \pm \frac{1}{r^2}\frac{B}{\sqrt{1/\xi^2 - N^2/r^2}},\end{aligned} \tag{36}$$

where the sign $+$ or $-$ is determined by whether it is outgoing ($\dot{r} > 0$) or in-going ($\dot{r} < 0$). For a null geodesic starting from and ending at asymptotic infinity, the point where it is closest to the compact object—namely, its turning point $r = r_{\rm tp}$—is obtained from the condition that $\dot{r} = 0$ there, which gives

$$\xi = \frac{r_{\rm tp}}{N(r_{\rm tp})}. \tag{37}$$

Then, the total deflection due to gravitational lensing $\Delta\phi_{\rm GL}(r_{\rm tp})$ of such a null geodesic—i.e., its deviation from a straight line—is given as [84]

$$\Delta\phi_{\rm GL}(r_{\rm tp}) = 2\left|\int_{r_{\rm tp}}^{\infty} \frac{{\rm d}r}{r^2}\frac{B(r)}{\sqrt{N^2(r_{\rm tp})/r_{\rm tp}^2 - N^2(r)/r^2}}\right| - \pi. \tag{38}$$

Within the current parametrization scheme, this may be rewritten as

$$\begin{aligned}&\Delta\phi_{\rm GL}(x_{\rm tp}) \\ &= 2\left|\int_{x_{\rm tp}}^{1} {\rm d}x \frac{B(x)}{\sqrt{(1-x_{\rm tp})^2 N^2(x_{\rm tp}) - (1-x)^2 N^2(x)}}\right| - \pi,\end{aligned} \tag{39}$$

where $x_{\rm tp} \coloneqq 1 - r_0/r_{\rm tp}$. This integral is finite only if the turning point lies outside the photon sphere—i.e., $x_{\rm ps} < x_{\rm tp} < 1$.

In the next section, we display the parameters necessary to parametrize various spacetimes based on the parametrization scheme described in Sec. II, and then proceed to demonstrate how efficiently metric functions and the various observables discussed in this section are characterized in this framework.

IV. CHARACTERIZING SPACETIMES AND OBSERVABLES IN THE PARAMETRIZATION SCHEME

We now discuss the conventions used here and the layout of this section before we enter into a brief description of the various BH, boson star, and naked singularity spacetimes considered in this work.

We employ geometrized units throughout: $8\pi G = c = 1$. Deviations in the gravitational constant G or the Planck length $l_{\rm p}$ can be measured in scales of their canonical values. Further, since the spacetimes considered here are all asymptotically flat, the ADM mass M can be used to fix a length scale for the Schwarzschild-like coordinate system used in Eq. (2). If we switch to a mass-dimensionless radial coordinate $\bar{r} = r/M$, a direct comparison of various quantities (observables and metric functions) associated with various solutions becomes meaningful.

This also allows us to obtain the dependence of various observables associated with the solutions considered here

TABLE I. Metric functions, $N^2(\bar{r})$ and $B^2(\bar{r})$, of the BH spacetimes from arbitrary theories of gravity that we have considered. Here, $\bar{r} = r/M$, and M is the ADM mass. The location of the Killing horizon $\bar{r}_0$ is obtained by solving $N^2(\bar{r}_0) = 0$, and is used in defining the conformal radial coordinate $x = 1 - \bar{r}_0/\bar{r}$. The patch of the spacetime that we capture within this parametrization scheme is the entire exterior horizon geometry, $0 \leq x < 1$. It is to be noted that for the Einstein-aether BHs, the Killing horizon is different from the actual causal boundary of the BH region. Also, the term $\bar{r}_-$ appearing in B^2 for the modified Hayward BH is the smaller zero of its N^2 metric function. We also show below the PPN-allowed range of the relevant parameter for each spacetime. Finally, in the last column we display the (rounded-up) maximum of the absolute values of all expansion coefficients for all PPN-allowed parameter values for a given spacetime, $\mathcal{L}^{\infty}_{\max}$, with its order of magnitude given in square brackets. This number is meant to provide a rough sense of the size of the region of this 11D parameter space on which a particular spacetime of astrophysical interest has support.

Spacetime	Physical charge	$N^2 = -g_{00}$	$B^2 = -g_{00}g_{11}$	PPN constrained	$\mathcal{L}^{\infty}_{\max}$
RN [57]	$0 < \bar{q} \leq 1$	$1 - \frac{2}{\bar{r}} + \frac{\bar{q}^2}{\bar{r}^2}$	1	$0 < \bar{q} \lesssim 2.1 \times 10^{-2}$	1 [−4]
E-ae 2 [62]	$0 < c_{13} < 1$, $0 \leq c_{14} \leq 2c_{13} < 2$	$1 - \frac{2-c_{14}}{\bar{r}} - \frac{(2c_{13}-c_{14})(2-c_{14})^2}{8(1-c_{13})}\frac{1}{\bar{r}^2}$	1	$0 < c_{13} < 1$, $0 \leq c_{14} \leq 2c_{13} < 2$	8 [−1]
E-ae 1 [62]	$0 < c_{13} < 1$	$1 - \frac{2}{\bar{r}} - \frac{3^3 c_{13}}{2^4(1-c_{13})}\frac{1}{\bar{r}^4}$	1	$0 < c_{13} < 1$	6 [−1]
Bardeen [58]	$0 < \bar{q}_{\rm m} \leq \sqrt{16/27}$	$1 - \frac{2\bar{r}^2}{(\bar{r}^2+\bar{q}_{\rm m}^2)^{3/2}}$	1	$0 < \bar{q}_{\rm m} \leq \sqrt{16/27}$	1 [1]
Hayward [59,60]	$0 < \bar{l} \leq \sqrt{16/27}$	$1 - \frac{2\bar{r}^2}{\bar{r}^3+2\bar{l}^2}$	1	$0 < \bar{l} \leq \sqrt{16/27}$	6 [0]
Bronnikov [68]	$0 < \bar{q}_{\rm m} \lesssim 1.05$	$1 - \frac{2}{\bar{r}}(1 - \tanh\frac{\bar{q}_{\rm m}^2}{2\bar{r}})$	1	$0 < \bar{q}_{\rm m} \lesssim 1.05$	2 [0]
EEH [69]	$0 < \bar{\alpha}$, $0 < \bar{q}_{\rm m}$	$1 - \frac{2}{\bar{r}} + \frac{\bar{q}_{\rm m}^2}{\bar{r}^2} - \bar{\alpha}\frac{2\bar{q}_{\rm m}^4}{5\bar{r}^6}$	1	$0 < \bar{\alpha}$, $0 < \bar{q}_{\rm m} \lesssim 2.1 \times 10^{-2}$	1 [0]
Frolov [61]	$0 < \bar{l} \leq \sqrt{16/27}$, $0 < \bar{q} \leq 1$	$1 - \frac{(2\bar{r}-\bar{q}^2)\bar{r}^2}{\bar{r}^4+(2\bar{r}+\bar{q}^2)\bar{l}^2}$	1	$0 < \bar{l} \leq \sqrt{16/27}$, $0 < \bar{q} \lesssim 2.1 \times 10^{-2}$	4 [0]
KS [63]	$0 < \bar{a}$	$-\frac{2}{\bar{r}} + \frac{\sqrt{\bar{r}^2-\bar{a}^2}}{\bar{r}}$	1	$0 < \bar{a} \lesssim 3.0 \times 10^{-2}$	4 [−1]
CFM A [64]	$\beta < 1$	$1 - \frac{2}{\bar{r}}$	$(1 - \frac{3}{2\bar{r}})(1 - \frac{4\beta-1}{2\bar{r}})^{-1}$	$\lvert\beta - 1\rvert \lesssim 2.3 \times 10^{-5}$	3 [0]
CFM B [64]	$1 < \beta < 5/4$	$1 - \frac{2}{\bar{r}}$	$(1 - \frac{3}{2\bar{r}})(1 - \frac{4\beta-1}{2\bar{r}})^{-1}$	$\lvert\beta - 1\rvert \lesssim 2.3 \times 10^{-5}$	3 [0]
Mod. Hayward [61]	$0 < \bar{l} \leq \sqrt{16/27}$	$1 - \frac{2\bar{r}^2}{\bar{r}^3+2\bar{l}^2}$	$\frac{\bar{r}^6+\bar{r}_-^6}{\bar{r}^6+\bar{r}_{\rm H}^4\bar{r}^2}$	$0 < \bar{l} \leq \sqrt{16/27}$	6 [0]
EMd [65–67]	$0 < \bar{q} \leq \sqrt{2}$	$1 - \frac{\sqrt{4\bar{r}^2+\bar{q}^4}-\bar{q}^2}{\bar{r}^2}$	$\frac{4\bar{r}^2}{4\bar{r}^2+\bar{q}^4}$	$0 < \bar{q} \lesssim 2.1 \times 10^{-2}$	2 [0]

on the other relevant physical "charges," like the scalar or electric or magnetic charge, etc. In instances when the mass of a compact object has been ascertained from observations to requisite precision, one could then potentially look for the dependence on other ADM charges of observational data. The mass scaling of the various observables considered here is clear from Sec. III. The impact parameter of a photon on an unstable circular orbit $\xi_{\rm ps}$, the orbital angular frequency for Kepler observers $\Omega_{\rm K}$, and the deflection angle due to gravitational lensing $\Delta\phi_{\rm GL}$ scale with mass as M, M^{-1}, and M^0, respectively. Further, since the conformal parameter x is scale invariant, the metric functions $N^2(x)$ and $B^2(x)$ are unaffected; i.e., changing the units of the radial coordinate does not affect the Padé expansion coefficients. This is an important quality that makes the definition of a parametrization space Π as in Sec. IV A useful.

For easy access, the BH metric functions used here have been compiled in Table I. We display in Table II the parametrization coefficients up to fourth order (ϵ, a_i, b_i for $0 \leq i \leq 4$) for all solutions considered here, BHs and otherwise. As discussed above, $n_0 = 0$ for BH spacetimes and $n_0 = \epsilon$ for non-BH spacetimes, since we set the inner boundary in these cases to correspond to the Schwarzschild radius, $\bar{r}_0 = 2$.

In the columns under part I of Table III, we show the relative error in obtaining $\xi_{\rm ps}$ and $\Omega_{\rm ISCO}$ for various spacetimes, when using Padé approximants truncated at the fourth order ($a_5 = b_5 = 0$), as an indicative quantitative measure of the "goodness" of the current parametrization scheme. For instance, for a Bardeen BH with specific magnetic charge $\bar{q}_{\rm m} = 0.75$, we find $|1 - \xi_{{\rm ph};a_5=0}/\xi_{\rm ph;\,exact}|$ to be 7.35×10^{-6}. We also show the maximum relative error in obtaining the metric functions $N^2(x)$ and $B^2(x)$ over the entire range $0 \leq x < 1$. Finally, we display also the maximum relative error in approximating the orbital angular frequency of Kepler observers $\Omega_{\rm K}$ and the deflection angle due to gravitational lensing $\Delta\phi_{\rm GL}$ over the entire accretion disk $x_{\rm ISCO} < x < 1$, where $x_{\rm ISCO}$ is defined via Eq. (35).

To compare the goodness of the present approximation, we show the *exact* relative differences from the Schwarzschild values of $\xi_{\rm ps}$ and $\Omega_{\rm ISCO}$ for various spacetimes under part II of Table III. For example, under the column for impact parameters, we report $|1 - \xi_{\rm ps;\,Spacetime}/\xi_{\rm ps;\,Schwarzschild}|$. We also show the relative error in obtaining

TABLE II. PPN and Padé approximant coefficients up to order 4 for various spacetimes. As discussed in the following Table III, at this order, the relative errors in obtaining both the metric functions and various observables is at the level of about 10^{-6}, and in fact systematically much lower for BHs. For the boson star and naked singularity, we have used $\bar{r}_0 = 2$, and so $n_0 = \epsilon$. On the other hand, for BHs, $n_0 = 0$. The parameter $\epsilon = 2/\bar{r}_0 - 1$ measures the difference of the horizon radius from its Schwarzschild radius for BHs. Also, as was discussed in Sec. III A above, ϵ, a_0, b_0 are the only relevant parameters to test whether a particular spacetime is "PPN allowed." Finally, if a Padé coefficient of some order n vanishes—i.e., if $a_{n\geq 1} = 0$ or $b_{n\geq 1} = 0$—then the corresponding metric function, N^2 or B^2, is exactly characterized within this approximation scheme at order n (see, e.g., the case of E-ae 1 BHs below).

		PPN coefficients (Taylor)			Higher-order a coefficients (Padé)				Higher-order b coefficients (Padé)			
Spacetimes	Physical Charge	ϵ	a_0	b_0	a_1	a_2	a_3	a_4	b_1	b_2	b_3	b_4
Schwarzschild	⋯	0	0	0	0	0	0	0	0	0	0	0
RN	$\bar{q} = 0.5$	0.07180	0.07180	0	0	0	0	0	0	0	0	0
	$\bar{q} = 0.9$	0.39286	0.39286	0	0	0	0	0	0	0	0	0
E-ae 2	[0.1, 0.1]	−0.01352	−0.01352	0	0	0	0	0	0	0	0	0
$[c_{13}, c_{14}]$	[0.9, 0.1]	−0.51007	−0.51007	0	0	0	0	0	0	0	0	0
	[0.9, 1.7]	−0.10102	−0.10102	0	0	0	0	0	0	0	0	0
E-ae 1	$c_{13} = 0.5$	−0.07666	0	0	0.07666	0	0	0	0	0	0	0
	$c_{13} = 0.9$	−0.26982	0	0	0.26982	0	0	0	0	0	0	0
Bardeen	$\bar{q}_{\rm m} = 0.25$	0.02471	0	0	0.00100	0.46236	−0.54081	0.04101	0	0	0	0
	$\bar{q}_{\rm m} = 0.75$	0.53960	0	0	0.32920	−0.07610	3.42051	−3.89389	0	0	0	0
Hayward	$\bar{l} = 0.25$	0.01641	0	0	−0.01561	−0.09932	0.70929	−0.40533	0	0	0	0
	$\bar{l} = 0.75$	0.33333	0	0	−0.08333	−3.75000	3.46667	−0.15897	0	0	0	0
Bronnikov	$\bar{q}_{\rm m} = 0.5$	0.07167	0.07178	0	0.00011	−0.00538	0.33468	−0.33299	0	0	0	0
	$\bar{q}_{\rm m} = 1.05$	1.03616	1.14273	0	0.08279	−0.36596	0.44373	−0.30767	0	0	0	0
EEH	[1, 0.05]	0.79539	0.80585	0	0.03140	1.00000	−0.66667	0.16667	0	0	0	0
$[\bar{q}_{\rm m}, \bar{\alpha}]$	[1,1]	0.48364	0.55030	0	0.19997	1.00000	−0.66667	0.16667	0	0	0	0
Frolov	[0.5, 0.25]	0.09732	0.07526	0	−0.02039	−0.15602	0.74279	−0.37350	0	0	0	0
$[\bar{q}, \bar{l}]$	[0.5, 0.6]	0.36454	0.11637	0	−0.09263	−2.39466	2.33431	−0.20990	0	0	0	0
	[0.9, 0.25]	0.61799	0.53013	0	−0.04369	−1.59541	1.85133	−0.17365	0	0	0	0
KS	$\bar{a} = 1$	−0.10557	−0.10000	0	0.00689	0.34416	0.32590	−0.22973	0	0	0	0
	$\bar{a} = 10$	−0.80388	−0.48077	0	2.97202	17.9580	8.72455	16.6646	0	0	0	0
CFM A	$\beta = -0.9$	0	0	−0.95000	0	0	0	0	0.29100	−0.80649	0.94227	1.09107
	$\beta = 0.9$	0	0	−0.05000	0	0	0	0	−0.10485	2.12935	0.03647	2.39174
CFM B	$\beta = 1.1$	0	0	0.05000	0	0	0	0	0.24099	4.93512	0.09874	4.23521
	$\beta = 1.2$	0	0	0.10000	0	0	0	0	1.13607	13.6579	1.56198	9.44727
Mod. Hayward	$\bar{l} = 0.25$	0.01641	0	0	−0.01561	−0.09932	0.70929	−0.40533	−0.00919	3.91749	−2.52087	0.52343
	$\bar{l} = 0.75$	0.33333	0	0	−0.08333	−3.75000	3.46667	−0.15897	−0.12939	2.05606	−3.40434	1.48027
EMd	$\bar{q} = 0.7$	0.15087	0.16225	0	−0.00011	0.48046	−0.52013	0.01976	−0.00979	−0.02928	0.49677	−0.50314
	$\bar{q} = 1.4$	6.07107	24.5000	0	−13.3186	−0.68426	0.05403	−0.99713	−0.72270	−1.64581	0.44380	−0.45354
MBS A	⋯	0.25607	−2860.02	0	2860.11	−0.99991	−0.00005	−1.03642	−0.33233	−0.54166	1.75930	−2.45991
MBS B	⋯	0.49436	−2860.02	0	2860.58	−0.99991	0.00007	−0.33170	−0.26234	−1.55777	0.57086	−0.71121
JNW	$\nu = 0.1$	0.59869	0	0	0.92739	−1.14757	0.14701	−0.58785	−0.86869	−1.82005	0.47494	−0.47888
	$\nu = 0.5$	0.22527	0	0	0.04698	3.34168	−4.35047	0.52143	−0.62883	−0.79818	1.41593	−1.78545
	$\nu = 0.9$	0.06345	0	0	−0.23279	2.18778	−2.43883	4.30862	−0.42314	4.60772	−3.49652	4.07833

TABLE III. Under part I of this table, we demonstrate the efficiency of the current parametrization scheme by reporting the maximum relative error, at fourth order, in approximating the metric functions of various metrics and the associated observables. Typically, the relative error drops by more than an order of magnitude, order on order, due to the use of Padé approximants (see Table V below), and at this order already the typical errors are at the level of 10^{-6}. Since this parametrization scheme converges rapidly with increasing order of approximation, those few entries that are of relatively low accuracy will be improved by adding a few higher-order coefficients. The convention we use below is that if a number is smaller than 10^{-10}, we set it to zero. For brevity, we display the order of magnitude within square brackets. Furthermore, since one of the objectives of such a parametrization scheme is to test theories of gravity, we think it useful to report the relative difference in the *exact* values of important observables for a particular spacetime from the corresponding values for the Schwarzschild BH, under part II; i.e., we use the exact metric functions for part II.

		I						II		
		Maximum relative error						Exact deviation from Schwarzschild		
		$\lvert\sigma\rvert = \lvert 1 - O_{\rm approx}/O_{\rm exact}\rvert$						$\delta = 1 - O_{\rm exact}/O^{\rm Schw}_{\rm exact}$		
Spacetime	Physical charge	$N^2[x]$	$B^2[x]$	$\xi_{\rm ps}$	$\Omega_{\rm ISCO}$	$\Omega_{\rm K}[x]$	$\Delta\phi_{\rm GL}[x]$	$\xi_{\rm ps}$	$\Omega_{\rm ISCO}$	$\Delta\phi_{\rm GL}(r_{\rm ISCO})$
RN	$\bar{q} = 0.5$	0	0	0	0	0	2.37 [−7]	4.39 [−2]	−8.21 [−2]	−6.67 [−2]
	$\bar{q} = 0.9$	0	0	0	0	0	1.12 [−7]	1.69 [−1]	−3.88 [−1]	−3.28 [−1]
E-ae 2	[0.1, 0.1]	0	0	0	0	0	2.95 [−8]	4.13 [−2]	−3.60 [−2]	1.27 [−2]
$[c_{13}, c_{14}]$	[0.9, 0.1]	0	0	0	0	0	7.42 [−8]	−6.71 [−1]	5.94 [−1]	4.87 [−1]
	[0.9, 1.7]	0	0	0	0	0	1.09 [−7]	8.39 [−1]	−4.86 [0]	9.61 [−2]
E-ae 1	$c_{13} = 0.5$	0	0	0	0	0	8.58 [−8]	−2.77 [−2]	4.98 [−2]	5.04 [−2]
	$c_{13} = 0.9$	0	0	0	0	0	1.49 [−7]	−1.55 [−1]	2.50 [−1]	2.43 [−1]
Bardeen	$\bar{q}_{\rm m} = 0.25$	0	0	0	1.49 [−9]	0	1.20 [−7]	1.06 [−2]	−2.16 [−2]	−2.10 [−2]
	$\bar{q}_{\rm m} = 0.75$	1.78 [−5]	0	7.35 [−6]	2.21 [−5]	1.33 [−5]	3.18 [−5]	1.20 [−1]	−2.86 [−1]	−2.92 [−1]
Hayward	$\bar{l} = 0.25$	4.77 [−7]	0	1.20 [−7]	2.56 [−6]	6.53 [−7]	8.89 [−6]	4.71 [−3]	−8.56 [−3]	−8.76 [−3]
	$\bar{l} = 0.75$	2.88 [−4]	0	1.29 [−4]	2.26 [−4]	2.28 [−4]	6.86 [−4]	5.03 [−2]	−9.25 [−2]	−9.65 [−2]
Bronnikov	$\bar{q}_{\rm m} = 0.5$	0	0	×	0	0	×	×	−8.20 [−2]	×
	$\bar{q}_{\rm m} = 1.05$	2.58 [−7]	0	×	2.95 [−8]	1.31 [−7]	×	×	−7.15 [−1]	×
EEH	[1, 0.05]	1.74 [−5]	0	×	4.44 [−7]	9.66 [−6]	×	×	−5.90 [−1]	×
$[\bar{q}_{\rm m}, \bar{\alpha}]$	[1, 1]	8.69 [−5]	0	×	2.22 [−4]	7.14 [−5]	×	×	−5.76 [−1]	×
Frolov	[0.5, 0.25]	1.01 [−6]	0	2.66 [−7]	4.37 [−6]	1.19 [−6]	2.54 [−6]	4.99 [−2]	−9.42 [−2]	−7.92 [−2]
$[\bar{q}, \bar{l}]$	[0.5, 0.6]	1.82 [−4]	0	7.87 [−5]	1.59 [−4]	1.41 [−4]	2.02 [−3]	8.34 [−2]	−1.63 [−1]	−1.51 [−1]
	[0.9, 0.25]	3.15 [−5]	0	1.47 [−5]	3.80 [−6]	1.94 [−5]	4.71 [−5]	1.83 [−1]	−4.27 [−1]	−3.70 [−1]
KS	$\bar{a} = 1$	2.74 [−7]	0	6.66 [−8]	1.45 [−6]	3.81 [−7]	8.68 [−7]	−7.82 [−2]	1.23 [−1]	9.86 [−2]
	$\bar{a} = 10$	1.70 [−2]	0	8.62 [−3]	4.34 [−2]	1.53 [−2]	2.38 [−2]	−2.59 [0]	8.81 [−1]	7.52 [−1]
CFM A	$\beta = -0.9$	0	1.16 [−3]	0	0	0	6.35 [−3]	0	0	7.28 [−1]
	$\beta = 0.9$	0	5.01 [−7]	0	0	0	3.38 [−7]	0	0	5.43 [−2]
CFM B	$\beta = 1.1$	0	5.40 [−6]	0	0	0	2.27 [−6]	0	0	−5.72 [−2]
	$\beta = 1.2$	0	1.87 [−3]	0	0	0	4.40 [−4]	0	0	−1.18 [−1]
Mod. Hayward	$\bar{l} = 0.25$	5.03 [−7]	2.93 [−4]	1.20 [−7]	2.56 [−6]	6.53 [−7]	2.78 [−4]	4.71 [−3]	−8.56 [−3]	−8.74 [−3]
	$\bar{l} = 0.75$	2.93 [−4]	4.73 [−3]	1.29 [−4]	2.26 [−4]	2.28 [−4]	2.60 [−3]	5.03 [−2]	−9.25 [−2]	−9.64 [−2]
EMd	$\bar{q} = 0.7$	0	9.69 [−9]	0	0	0	7.54 [−8]	8.67 [−2]	−1.72 [−1]	−1.37 [−1]
	$\bar{q} = 1.4$	1.76 [−2]	2.21 [−2]	7.22 [−3]	6.84 [−3]	4.71 [−3]	3.77 [−2]	5.36 [−1]	−3.18 [0]	−3.19 [0]
MBS A	⋯	3.85 [−4]	2.01 [−2]	×	×	0	⋯	×	×	×
MBS B	⋯	5.09 [−2]	5.95 [−2]	×	×	0	⋯	×	×	×
JNW	$\nu = 0.1$	2.10 [−3]	4.30 [−2]	×	×	5.64 [−3]	1.57 [−2]	×	×	×
	$\nu = 0.5$	2.00 [−3]	4.54 [−3]	×	7.81 [−3]	9.53 [−4]	9.21 [−4]	×	4.14 [−1]	1.80 [−1]
	$\nu = 0.9$	1.40 [−3]	3.50 [−3]	6.95 [−4]	1.11 [−3]	6.65 [−4]	2.91 [−4]	1.18 [−2]	1.88 [−2]	7.72 [−3]

the deflection angle due to gravitational lensing at the ISCO radius $\Delta\phi_{\rm GL}(r_{\rm ISCO})$ there.

Since the relative error levels in obtaining the exact observables within this parametrization scheme are significantly lower when compared to the deviation of their exact values from the Schwarzschild spacetime, setting up precision tests is possible. Furthermore, since the number of parameters to characterize the wide variety of compact objects in use here is small (only 11), we conclude that this parametrization scheme is a promising framework to test theories of gravity and the quantum-field-theoretic effects that may show up in astrophysical data related to compact objects. It is remarkable that this parametrization method performs quite well across the entire radial patch, and it allows one to capture both weak and strong gravitational field regimes simultaneously.

A. Parametrization space Π

We now introduce the geometric notion of a parametrization space. If we think of each set of PPN and Padé expansion coefficients $(\epsilon, a_{0\le i\le 4}, b_{0\le i\le 4})$ as being points of some abstract "parametrization space" Π, then it is clear that for each set of physical charges q_j for a given spacetime, we can associate a point $\pi(q_j) \in \Pi$. As we vary the physical parameters q_j associated with that particular spacetime over its entire range, we obtain a curve or surface in Π, depending on the number of charges $q_1, q_2 \ldots q_j$. We can then use the usual Euclidean $\mathcal{L}^2$-norm on Π to measure distances between such curves or surfaces, or equivalently between solutions. In particular, we define the deviation of a solution from the Schwarzschild BH spacetime, which sits at the origin of this space, as simply being given by

$$\mathcal{L}_0^2 \coloneqq (\pi - 0)^2 = \left(\epsilon^2 + \sum_{i=0}^{4}(a_i^2 + b_i^2)\right)^{1/2}. \quad (40)$$

Table II then lists the coordinates of various spacetimes in this space. When two "solution curves" intersect, the corresponding spacetimes match approximately at the common point. It is to be noted that since we have used only the first few $(n \le 4)$ expansion coefficients to set up Π, various spacetimes are approximated at varying degrees of accuracy. However, since a higher-order approximation does not affect low-order PPN or Padé coefficients, we can always compare spacetimes meaningfully on Π. For an alternative prescription to measure differences between solutions, one may see Ref. [85], where a superspace approach was adopted.

Now, for each solution, we use a grid with 1000 points for each physical charge, and we obtain the PPN and Padé coefficients $\pi(q)$ at each grid point q. For the Bardeen BH, there is a single physical parameter $\bar{q}_{\rm m}$, and we obtain $\pi(\bar{q}_{\rm m})$ for 1000 points within $0 \le \bar{q}_{\rm m} \lesssim .76$. We then ascertain whether the PPN constraints [Eq. (18)] are met at each grid point and thus obtain the PPN-allowed parameter values for each spacetime. This is reported in Table I. We introduce another useful quantity, the $\mathcal{L}^\infty$-norm, which is defined as

$$\mathcal{L}^\infty \coloneqq \max\{|\epsilon|, |a_i|, |b_i| (0 \le i \le 4)\}, \quad (41)$$

to characterize deviations from the Schwarzschild BH solution and obtain its value at each grid point for a particular spacetime. We can then find the maximum value of $\mathcal{L}^\infty_{\rm max}$ over all the (PPN allowed charge) grid points for a particular spacetime, to obtain a measure of the extent of the region in Π on which the spacetime has support. Since all of these solutions become approximately Schwarzschild in the limit of approach to a particular physical parameter value, as can be seen from Table I, $\mathcal{L}^\infty_{\rm max}$ gives a sense of the maximal deviation from the Schwarzschild BH solution. Essentially, if one samples this range of the parameter space along all axes, one is sure to have characterized that particular spacetime. We report $\mathcal{L}^\infty_{\rm max}$ for each spacetime in the last column of Table I for BHs. Note that for all of the spacetimes considered here, this quantity $\mathcal{L}^\infty_{\rm max}$ is finite. That is, by sampling the region $0 < |\epsilon|, |a_i|, |b_i| (0 \le i \le 4) < 10$, we have completely characterized all of the BH spacetimes used in this work. Of course, since the exact value of $\mathcal{L}^\infty_{\rm max}$ depends on the resolution of the grid, we report here a rounded-up value as an indicative measure.

For the JNW naked singularity spacetime, we obtain $\mathcal{L}^\infty_{\rm max} \approx 26$. (We use a very coarse grid, $\nu = 0.1, 0.2, \ldots, 0.9$, for this spacetime.) For each of the boson star models considered here, this number appears to be around $\mathcal{L}^\infty_{\rm max} \approx 10^3$. What this means is that all of the spherically symmetric metrics used here lie in a compact region of Π around the origin.

Note that we will not restrict our study to the PPN-allowed ranges of the physical charges for the BH spacetimes, reported in Table I, but explore their entire ranges instead.

B. Black holes

Note that since the mass M is the ADM mass for all of the solutions below, and is a free parameter, we will only discuss the remaining charges in what follows.

The Reissner-Nordström (RN; Ref. [57]) BH describes a charged BH in GR, with specific charge $0 < \bar{q} \le 1$.

We consider two BH solutions reported in Ref. [62] that are obtained from the Einstein-aether (E-ae) Lagrangian. In an aether theory, LLI is violated due to the existence of the aether vector field. The first of the two solutions, which we call the E-ae 1 BH is a single-parameter solution, $0 < c_{13} < 1$, and the E-ae 2 solution represents a two-parameter family of BHs which take the values $0 < c_{13} < 1$ and $0 \le c_{14} \le 2c_{13} < 2$. Here, c_{13} and c_{14} are coupling constants that control the aether Lagrangian. It is to be noted that for these spacetimes, the causal horizons that separate the BH interiors $B \equiv M - J^-(I^+)$ from their exteriors, called the universal horizons in Ref. [62], are different from Killing horizons, and we use the latter when defining the conformal coordinate x.

The Einstein-gravity Lagrangian—when coupled to a particular nonlinear electrodynamics (NLED) Lagrangian $\mathcal{L}(F)$, which reduces to Maxwell in the weak-field limit, with F being the electromagnetic field strength scalar [see Eq. (29) of Ref. [68]; see also Ref. [55]]—yields regular, magnetically charged BH solutions. These Bronnikov BH solutions are given by Eqs. (3), (11), and (30) of Ref. [68], with the specific magnetic charge $0 < \bar{q}_{\rm m} \lesssim 1.05$ as the only additional charge.

When considering the Einstein Lagrangian coupled to the Euler-Heisenberg (EH) NLED Lagrangian, which is

considered to be an effective action of a superstring theory [86], one can obtain a magnetically charged BH solution [69]. This Einstein-Euler-Heisenberg (EEH) BH depends on two parameters, $0 < \bar{\alpha}$ and $0 < \bar{q}_{\rm m}$, the former of which is the coupling constant of the F^2 piece of the EH Lagrangian and is expected to be determined by the string tension α' [69].

It is important to note that due to the self-interaction introduced by the nonlinearity of the NLED Lagrangians in the Bronnikov and the EEH BH solutions, photons do not propagate along null geodesics of Eq. (2) (see, e.g., the discussion in Ref. [87]). However, as was discussed in Ref. [88], the event horizons are still determined by the zeroes of the null expansions of Eq. (2). Therefore, our definition of the conformal coordinate x is unchanged, and we can still characterize these BH spacetimes within the current parametrization scheme. However, other important phenomena such as geometric redshift and light deflection are modified by the NLED Lagrangian. While we are able to show that these solutions are obtained within our parametrization scheme to very high accuracy, and also show that the errors in obtaining the ISCO frequency and the Kepler frequency are also very small (matter is still minimally coupled), we find studying the accuracy in obtaining the photon sphere impact parameter or the deflection of photons due to gravitational lensing for these spacetimes to be beyond the scope of the current article.[6]

The Bardeen BH model, proposed in Ref. [58], is the result of the collapse of charged matter, with the usual central singularity replaced by a regular charged matter core. The only relevant parameter in this solution takes values $0 < \bar{q}_{\rm m} \lesssim 0.77$. More recently, it was shown in Ref. [91] that this BH can also be obtained as an exact magnetically charged solution of an Einstein-NLED Lagrangian.

The Hayward BH model [59] proposes a method to resolve the central singularity in uncharged BHs in GR by adding a region with positive cosmological constant $\Lambda = 3/l^2$ (de Sitter) close to the center, where l is the Hubble length. Such a model is expected to be justified by the properties of matter [92,93] or the quantum theory of gravity [94–97] close to the center of the BH. While l provides a length scale for when such effects might set in, and can therefore be related to the Planck length, larger length scales are not strictly excluded. We will consider here the entire range of the parameter for which BH solutions are admitted, $0 < \bar{l} \lesssim 0.77$. Since we have introduced the ADM mass into the definition of $\bar{l}$, which can be determined in terms of the canonical values of G and c, fixing a particular length scale l can be thought of equivalently as considering BHs within a certain mass range.

The charged generalization of the Hayward model given by Eq. (4.1) of Ref. [61] is referred to as the Frolov BH here and has an additional parameter which takes values $0 < \bar{q} \leq 1$. Another generalization of the Hayward model is also presented there, which modifies the redshift function in Eqs. (2.47) and (2.50); this we refer to as the modified Hayward model.

The effective dynamics of spherically symmetric fluctuations of the 4D gravitational field can be shown to be governed by a 2D dilaton gravity action [63]. By integrating out these fluctuations, one can obtain the (approximate) Kazakov-Solodhukin (KS) BH metric, given in Eq. (3.18) of Ref. [63]. The relevant parameter for this solution takes values $0 < a$ and determines the area of the singular two-sphere—i.e., $\mathcal{A}_{\rm sing} = 4\pi a^2$. While this parameter should be roughly of the order of the Planck length, we allow it to take all positive values here. While, more significantly, nonsingular solutions are also presented there, we do not consider them here.

Projecting the 5D vacuum Einstein equations onto a timelike manifold of codimension 1 (brane) yields the usual ADM Hamiltonian and momentum constraints for spherically symmetric solutions. If one chooses the four-metric on the brane to be given by Eq. (2) with $N^2(\bar{r}) = (1 - 2/\bar{r})$, this Hamiltonian constraint equation uniquely determines the other metric function, and a one-parameter family of Casadio-Fabbri-Mazzacurati (CFM) BH solutions are obtained, given in Eq. (8) of Ref. [64]. For $\beta < 1$, these are singular (CFM A), and for $1 < \beta < 5/4$, these are nonsingular (CFM B). The CFM B BHs in fact contain traversable wormholes (the minimal sphere is behind the horizon; see Fig. 2 of Ref. [64]). The parameter β here corresponds exactly to the PPN β parameter.

Due to the coupling of the dilaton field to the electromagnetic field strength $\boldsymbol{F}$ in heterotic string theory, the Einstein-Maxwell-dilaton (EMd) BH is the appropriate electromagnetically charged BH solution in the low-energy limit for this theory [65–67], as opposed to the RN BH. The EMd BH is characterized by the boundary value of the dilaton field ϕ_0 and the specific electric or magnetic charge $\bar{q}$. For convenience, we consider here solutions with $\phi_0 = 0$. In this case, EMd BH solutions exist for $0 < \bar{q} \leq \sqrt{2}$.

All BH solutions (barring the NLED BHs, which we have not studied here) cast shadows, and all BH solutions admit ISCOs.

C. Boson stars

Spherically symmetric solutions of the Einstein-Klein-Gordon Lagrangian with a quadratic potential can be used to model mini–boson stars (MBSs; Ref. [98]). Since the

[6]In the case of the Bronnikov BH, while it has been discussed that NLED photons propagate along the null geodesics of an effective metric given in Eqs. (26) and (27) of Ref. [68] (see also Refs. [89,90]), this supplementary "optical metric" is plagued by coordinate and curvature singularities, and the causal structure of this spacetime is unclear to us.

matter (scalar field) constituting the MBSs, in principle, extends all the way to infinity, albeit with the scalar field density decaying rapidly, these objects lack a sharp boundary or surface, and also permit stable circular orbits all the way to the center of the spacetime. MBSs can be extremely compact, with the 99% compactness parameter $\mathcal{C}_{99} = M_{99}/R_{99}$ reaching values of about 0.08, where R_{99} is the radius within which 99% of the mass (M_{99}) is contained. This parameter is a good measure of how compact an astrophysical object without a surface is; to compare, for a Schwarzschild BH, this value is 0.5. Here, we use the two MBS models, denoted A and B, that were numerically obtained and studied in Ref. [21]. These have compactnesses of 0.064 and 0.07, and they lie on the unstable and stable boson star branches, respectively. Since from about a few tens of Schwarzschild radii, these spacetimes look identical to that of the Schwarzschild BH, the associated PPN parameters β and γ are identical to the Schwarzschild BH values. Also, these models lack photon spheres and regions close to the center contribute to the image of the boson star [21]. However, it is discussed there that due to lower densities at the center in these models, a relatively dark region may be discernible.

D. The Janis-Newman-Winicour naked singularity

The Janis-Newman-Winicour (JNW) spacetime is also obtained as a solution of the Einstein-Klein-Gordon Lagrangian [70] and can be expressed more simply, as in Ref. [99]. The JNW solution, when written in the form given in Eq. (1), has metric functions [99],

$$f(\rho) = g^{-1}(\rho) = \left(1 - \frac{2M}{\rho\nu}\right)^{\nu}, \quad h(\rho) = \rho^2\left(1 - \frac{2M}{\rho\nu}\right)^{1-\nu}. \tag{42}$$

The parameter ν governs the strength of the scalar field and is given in terms of the specific scalar charge $\bar{\Phi}$ as $\nu = (1+\bar{\Phi}^2)^{-1/2}$. Clearly, depending on the strength of the scalar field, $0 < \nu < 1$. The JNW spacetime contains a strong curvature singularity at $\rho = 2M/\nu$, which can be seen by computing its Kretschmann scalar $\mathcal{K} = R^{abcd}R_{abcd}$, which diverges there.[7]

It can be straightforwardly seen that $h(\rho)$ is a bijective function (in fact, it is monotonically increasing) for all ν, which allows us to recast the JNW metric into the presently desired form [Eq. (2)]. In terms of the polar-areal radial coordinate r, it can be verified that the curvature singularity is now at $r = 0$ and has zero proper area.

[7]It is useful to check both the Ricci and Kretschmann scalars, since the Ricci and Weyl scalars are known to remain finite for several types of solutions containing curvature singularities. For example, Ricci vanishes for electrovacuum solutions, and Weyl vanishes for any conformally flat spacetime [100].

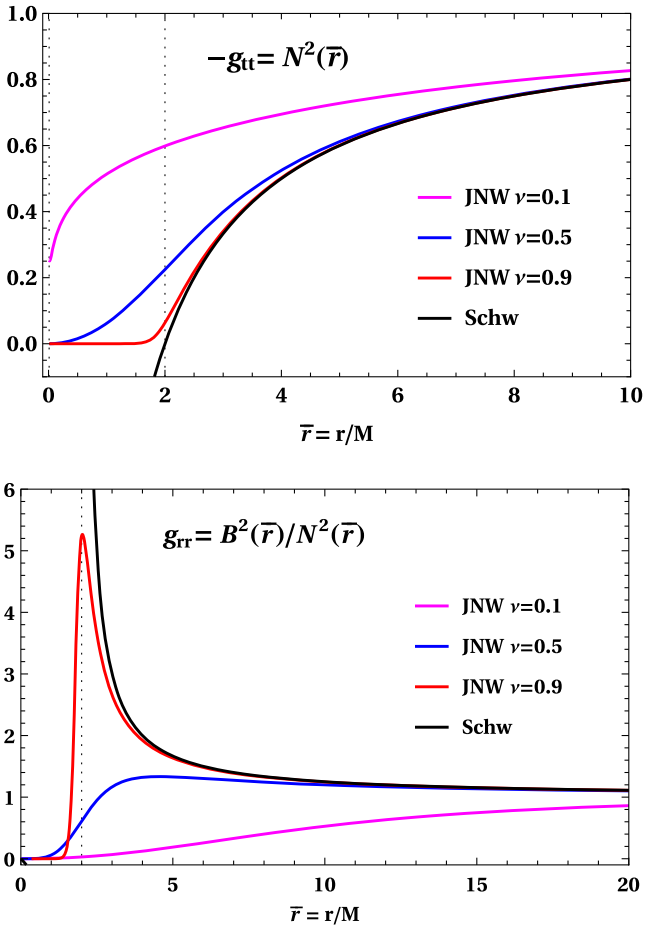

FIG. 1. We show here the metric functions $g_{tt} = -N^2(\bar{r})$ and $g_{rr} = M^2B^2(\bar{r})/N^2(\bar{r})$ for the JNW naked singularity spacetime for various values of the scalar field parameter, $\nu = 0.1, 0.5, 0.9$. The strength of the scalar field grows with decreasing ν. We also show these metric functions for the Schwarzschild BH for comparison. For both spacetimes, we have set $M = 1$.

Since the coordinate transformation equation [Eq. (3)] for the JNW spacetime,

$$\bar{\rho}^2\left(1 - \frac{2}{\bar{\rho}\nu}\right)^{1-\nu} = \bar{r}^2, \tag{43}$$

is typically transcendental in nature, we solve for $\bar{\rho}(\bar{r})$ numerically. In the above, we have switched to dimensionless coordinates, $\bar{\rho} = \rho/M$ and $\bar{r} = r/M$. For values of $\nu = 0.1, 0.3, \ldots, 0.9$, we use a uniform grid in $\log \bar{r}$, with 100 points per decade to solve Eq. (43). For these values, Eq. (43) reduces essentially to finding the roots of a high-degree polynomial. The grid extends from an outer radius $\bar{r}_{\rm max} = 10^7$ down to an inner radius $\bar{r}_{\rm min} = 10^{-2}$. The inner grid point is sufficiently small for our purposes, since we are interested in the radial range $2 \leq \bar{r} < \infty$.

It has been shown that this spacetime contains a photon sphere for $0.5 < \nu$ [101]. For $1/\sqrt{5} \leq \nu < 0.5$, two

timelike marginally outer/inner stable circular orbits exist at $\bar{r}_{\rm osco}$ and $\bar{r}_{\rm isco}$; stable circular orbits extend all the way from the center to $\bar{r} = \bar{r}_{\rm osco}$ and from $\bar{r} = \bar{r}_{\rm isco}$ to infinity. For $0.5 \leq \nu < 1$, a single marginally stable circular orbit remains at $\bar{r} = \bar{r}_{\rm isco}$, and stable circular orbits exist only outside this location. Using the results of Refs. [101,102], we can find the locations of the photon sphere and the timelike marginally stable circular orbits in polar-areal radial coordinates to be

$$\bar{r}_{\rm ps} = \left(\frac{1+2\nu}{\nu}\right)\left(1-\frac{2}{1+2\nu}\right)^{\frac{1-\nu}{2}},$$
$$\bar{r}_{\rm isco/osco} = \left(\frac{1+3\nu \pm \sqrt{5\nu^2-1}}{\nu}\right) \times \left(1-\frac{2}{1+3\nu\pm\sqrt{5\nu^2-1}}\right)^{\frac{1-\nu}{2}}. \quad (44)$$

In obtaining the above, we have simply used Eq. (43). We are able to numerically recover $\bar{r}_{\rm ps}$ and $\bar{r}_{\rm isco}$ with a relative error of about 10^{-6} from the exact values reported in Eq. (44). Note, however, that we are unable to obtain the photon sphere or ISCO radius when $\bar{r}_{\rm ps}, \bar{r}_{\rm isco} < \bar{r}_{\rm min}$. This, however, corresponds to a very small range of $0 < \nu < 1$. Since the JNW metric has not (commonly) been reported in polar-areal coordinates, we think it useful to display its metric functions for various values of the scalar field parameter ν and $M = 1$ in Fig. 1.

Once we obtain $N^2(\bar{r})$ and $B^2(\bar{r})$, we make the final change of coordinates to $x = 1–2/\bar{r}$ and obtain the parametrization coefficients, which we report in Table II. Finally, it can be checked that the PPN parameters β and γ for this spacetime vanish identically for all ν.

V. DISCUSSION AND SUMMARY

We have proposed here an extension to the RZ parametrization scheme to allow for the characterization of arbitrary asymptotically flat, spherically symmetric spacetimes, including those of stars and naked singularities. Within this scheme, we obtain highly accurate values for the metric functions for a variety of spacetimes: singular and nonsingular BHs from general relativity, BHs from the Einstein-aether theory, black holes from general relativity coupled to nonlinear electrodynamics, string-inspired BH and wormhole solutions, and mini–boson stars and naked singularities in general relativity. Various other BH solutions (including some here) have already been studied within this parametrization scheme, and its efficiency in obtaining various observables has been well established [103–105] (see also Ref. [71] and references therein). Recently, an extension of the RZ parametrization framework to characterize spherically symmetric BHs in higher dimensions has also been proposed [106].

The shadow radii $\xi_{\rm ph}$ of compact objects and the Kepler orbital angular velocities $\Omega_{\rm K}$ of matter in the accretion disks around them depend only on the g_{tt} component of the corresponding metric. Therefore, accurate measurements of these observables could be translated into constraints on the ϵ and a parameters considered here. Additionally, the profile of the gravitational lensing angle $\Delta\phi_{\rm GL}(r)$ for photons emitted from the accretion disk region depends also on the g_{rr} component, and when combined with the other observables used here, could constrain the entire metric of spherically symmetric (or slowly rotating) astrophysical compact objects. Other observables, such as the quasinormal frequencies associated with a compact object, also depend on both metric functions (see Eq. 49 of Ref. [51] for scalar perturbations), and combined constraints coming from all of these observables can be simultaneously imposed in the present framework to potentially test the underlying theories of gravity.

We have shown above that by sampling the region $0 < \epsilon, |a_i|, |b_i| (0 \leq i \leq 4) < 10$, we have completely characterized all of the BH spacetimes used in this work (when PPN constraints are met). This is useful when attempting to solve the inverse problem of reconstructing a metric function approximately given a set of observables that can essentially be determined in terms of these variables, or equivalently as functions over Π. Note, however, that these parameters may not be chosen freely. For example, for BHs the conditions $\epsilon > -1$ and $A(x) > 0$ over $0 < x < 1$ must always be satisfied.

If the exact relative difference in an observable O for a spacetime from its Schwarzschild BH value O^0 is given as $\delta = 1 - O/O^0$, and the relative error in approximating the value of O is given by $\sigma = 1 - O_{\rm approx}/O$, then

$$\delta_{\rm approx} \equiv 1 - \frac{O_{\rm approx}}{O^0} = \delta + \sigma(1-\delta), \quad (45)$$

and so the absolute error in obtaining δ is

$$\delta_{\rm approx} - \delta = \sigma(1-\delta). \quad (46)$$

Note that δ need not be a small number; for spacetimes that deviate significantly from the Schwarzschild BH, δ can be large (see Table III). However, the absolute error in obtaining δ due to approximation is clearly controlled by σ. As we can see from Table III, where we display both $|\sigma|$ and δ, for the spacetimes considered here, $|\sigma|$ is systematically low, about 10^{-6}. For various spacetimes, it is significantly lower. This means that the error in determining whether a particular spacetime is different, and how different it is, from the Schwarzschild BH using EHT observables within the present parametrization scheme is appreciably low. Since this framework employs Padé approximants, the typical order-on-order decrease in $|\sigma|$ is about $10^{-1} - 10^{-2}$, as can be seen from Fig. 2 of Appendix B below. Therefore, we are able to argue

comfortably that the current framework is useful to visualize and compare various spacetimes (in terms of the parametrization space Π introduced above), to characterize various strong-field observables associated with them, and to enable efficient tests of both properties of BHs from general relativity and GR itself.

Various BH solutions considered here [58,59,62–69] were recently studied within the same framework [51] at first and second order in Padé expansion [71]. It was reported there that all of these solutions, for moderate deviations from the Schwarzschild solution, are well approximated already at second order. While our findings are consistent with those of Ref. [71], since the aim of the present study is to explore the entire parameter range for these BH solutions, and errors within this parametrization scheme typically grow with deviation from Schwarzschild (as can be seen from Table III above and Table IV in Appendix C below), it becomes imperative that we consider higher-order approximations. As has been discussed above, we find that at the fourth order, errors in approximating metric functions and observables are sufficiently low across the entire parameter range for all BH solutions. Furthermore, our PPN constraint study shows that many of the BH spacetimes considered here (Bardeen, Hayward, modified Hayward) satisfy the PPN constraints across their entire parameter range (see Table I), and parametrizing BHs that deviate significantly (close to their maximal deviation, even) from the Schwarzschild solution becomes important from an observational standpoint. Also, to bring the error in approximating the deflection angle due to gravitational lensing $\Delta\phi_{\rm GL}(r)$ across the entire accretion disk $r_{\rm ISCO} \leq r$ to sufficiently low levels, we find a fourth-order approximation to be typically necessary. A comparison of the errors reported in Ref. [71] with those reported here when approximating the ISCO orbital angular velocity $\Omega_{\rm ISCO}$ also demonstrates the rapidity of the convergence to the true value by going to higher orders within the current framework, due to its use of Padé approximants. The relative error levels $|\sigma|$ reported here are typically a few orders of magnitude smaller than the ones reported in Ref. [71], as can be seen from Table V of Appendix C below. For example, the errors in approximating $\Omega_{\rm ISCO}$ or the common BH solutions vary between 0.2%–10.5% at first order and between 0.04%–7.95% at second order [71], while the maximum percentage error at fourth order is about 10^{-4}% for moderate deviations from the Schwarzschild solution. Finally, we think it useful to note that while we have focused on approximating observables that are associated with the construction of the image of a compact object, a study of the quasinormal frequencies associated with scalar perturbations of these BH spacetimes, which could be indicative of their gravitational wave frequency spectrum, is also presented in Ref. [71].

We note two limitations of this framework: First, spacetimes that have identical metric functions on $\bar{r}_0 \leq \bar{r} < \infty$ cannot be distinguished between. For example, thin-shelled gravastars [107], whose exterior geometries are described by the Schwarzschild metric, are hard to distinguish from a Schwarzschild black hole in this parametrization scheme. The second limitation is that if a metric is nonanalytic—i.e., if the metric functions or, as is more common, their derivatives have discontinuities at some surface—then they cannot be well characterized within this framework across the entire range over which the metric is defined. Of course, the patch outside the discontinuous surface can still be well characterized. Note that a metric derivative discontinuity does not imply that the spacetime is unphysical; this is a common feature of various solutions that describe the collapse of matter, and of the eventual limiting spherically symmetric spacetimes they settle into. In these scenarios, the spacetime is divided into two regions depending on the extent of the matter, with the interior collapsing region matched to an appropriate exterior metric. While the first and second fundamentals of such a spacetime (induced metric and extrinsic curvature) are smoothly matched, the spacetime metric could still present discontinuities on the matching surface (see, for example, Ref. [20]). In such cases, it might be possible that a two-point or even a multipoint Padé-approximant-based approach would yield dividends (see, for example, Sec. 8.3 of Ref. [76] for a discussion, and for related numerical results).

Finally, we note that the low level of errors in obtaining the metric functions up to two derivatives (see Table IV below) serves as a serious impetus to attempt a study of hydrodynamics within this framework, and potentially obtain full general-relativistic magnetohydrodynamic (GRMHD) simulations of accretion flows around various compact objects with state-of-the-art codes such as the Black Hole Accretion Code (BHAC) [108,109], for instance. In fact, for the Einstein-dilaton BH spacetime (discussed here) GRMHD simulations have already been successfully implemented [110], where it has been shown that there are clear observational differences in its image from that of a GR Kerr BH. Another potential application would be to study tidal disruptions of stars and neutron stars close to compact objects. While we do not display here the errors in obtaining the curvature invariants $R = R^{ab}R_{ab}$ and the Kretschmann scalar $\mathcal{K} = R^{abcd}R_{abcd}$, we find that these are also typically approximated very well within this parametrization scheme, as can be expected from the errors in the values of the metric and its derivatives reported here. This implies that one can calculate the Weyl scalar efficiently as well and potentially characterize the radii of tidal disruption events for various spacetimes by introducing a Frenet-Serret tetrad along static observers (see, for example, Ref. [82] and references therein), to provide yet another new observable to distinguish solutions. While the spectrum of quasinormal modes of scalar [71,111] and axial gravitational [112] perturbations of spacetimes within this scheme has been studied and is somewhat

representative of the spectrum of gravitational waves (GWs), a study of the latter requires one to consider the equations of motion of the theory of gravity that the spacetime belongs to. Since we show that the error in approximating up to second derivatives of the metric function across the entire exterior geometry is small already at the fourth order in our framework, it is possible that the GW spectra of higher-derivative gravity theories can also be obtained efficiently in this framework.

ACKNOWLEDGMENTS

It is a pleasure to thank Enrico Barausse, Hector Olivares, Ronak M. Soni, and Sebastian Völkel for useful discussions. Support comes in part from the ERC Synergy Grant "BlackHoleCam: Imaging the Event Horizon of Black Holes" (Grant No. 610058).

APPENDIX A: TORTOISE COORDINATE FOR BLACK HOLE SPACETIMES

If the metric $\boldsymbol{g}$ of a spacetime can be brought into the form $\boldsymbol{g}(\boldsymbol{x}) = \mathcal{C}(\boldsymbol{x})\boldsymbol{\eta}$, then such a metric $\boldsymbol{g}$ is conformally flat, and the coordinates x^μ are called conformally flat coordinates; here $\boldsymbol{\eta}$ is the Minkowski metric tensor. Such coordinates are particularly useful when attempting to study the global causal structure of a spacetime. Radial null geodesics in the associated spacetime diagrams are given by 45° lines, similar to flat-space spacetime diagrams.

Since all 2D geometries are conformally flat, we can find them for the $t-r$ plane of arbitrary BH ($n_0 = 0$) spherically symmetric metrics [Eq. (2)] as

$$\begin{aligned} \mathrm{d}s^2_{d\theta=d\phi=0} &= -N^2(r)\left(\mathrm{d}t^2 + \frac{B^2(r)}{N^4(r)}\mathrm{d}r^2\right) \\ &= -N^2(r)(\mathrm{d}t^2 + \mathrm{d}r_*^2), \end{aligned}$$

where the equation to achieve the coordinate transformation $r \to r_*$ can be read off from above as

$$\frac{dr_*}{dr} = \frac{B(r)}{N^2(r)}. \tag{A1}$$

In terms of the function A defined in Eq. (5) above, this is simply

$$\frac{dr_*}{dr} = \left(1 - \frac{r_0}{r}\right)^{-1}\frac{B(r)}{A(r)}. \tag{A2}$$

For the Schwarzschild spacetime, since $A(r) = B(r) = 1$, this coordinate $-\infty < r_* < \infty$ is exactly the familiar tortoise coordinate,

$$r_* = r + r_0 \ln\left|1 - \frac{r_0}{r}\right|. \tag{A3}$$

We can now relate the two conformal coordinates, x and r_*, for a generic BH spacetime, via

$$\frac{dr_*}{dx} = \frac{r_0}{x(1-x)^2}\frac{B(x)}{A(x)}. \tag{A4}$$

APPENDIX B: COMPARISON WITH THE CARSON-YAGI PARAMETRIZATION SCHEME

The metric of a spherically symmetric ($S = 0$) BH spacetime in the Carson-Yagi (CY) parametrization scheme [77] can be expressed as

$$\begin{aligned} \mathrm{d}s^2 = &-\left(1 - \frac{2M}{r}\right)A_1^{-2}(r)\mathrm{d}t^2 + \left(1 - \frac{2M}{r}\right)^{-1}A_5^{-1}(r)\mathrm{d}r^2 \\ &+ r^2\mathrm{d}\Omega_2^2, \end{aligned} \tag{B1}$$

where the functions $A_1(r)$ and $A_5(r)$ measure the deviation of an arbitrary BH metric from Schwarzschild. An asymptotic Taylor expansion for these functions is then employed to characterize them as

$$A_i(r) = 1 + \sum_{n=1}^{\infty}\alpha_{i0}\left(\frac{M}{r}\right)^n. \tag{B2}$$

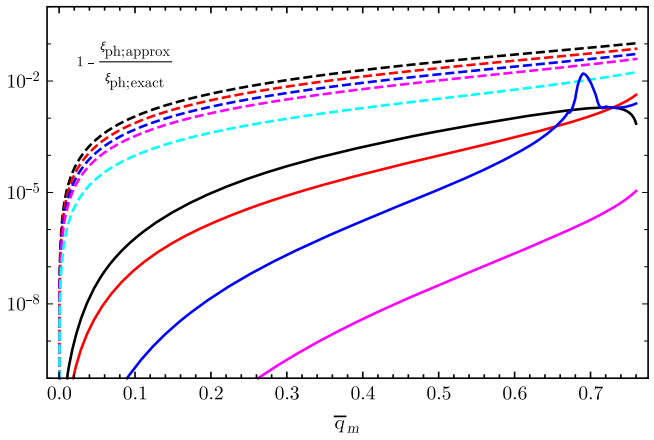

FIG. 2. We consider here the Bardeen BH [58], with specific magnetic charge $0 < \bar{q}_{\rm m} \lesssim 0.77$, and show the absolute relative error in estimating the exact value of its unstable circular photon-orbit impact parameter $\xi_{\rm ps;exact}$ within the Carson-Yagi parametrization scheme (in dashed lines), which uses Taylor expansions to characterize metric functions, and in our scheme, which uses expansions of Padé approximants. Considering α_{13} to be the first nontrivial parameter of the CY approximation scheme, lines in the same color correspond to the same number of approximation parameters. To be clear, dashed black and solid black correspond to the $\alpha_{1i>13} = 0$ Carson-Yagi and $a_{i>2} = 0$ Padé approximations, respectively. We also show in dashed cyan the seventh-order CY relative error—i.e., for $\alpha_{1i>19} = 0$. It is apparent that the Padé approximation does better already at first order relative to the seventh-order Taylor expansion. Note also that the rapidity of convergence is much higher when employing Padé approximants.

To compare the rapidity of the convergence of this scheme against the one used in the current work, we study the Bardeen-BH spacetime [58]. For this BH, we obtain the CY functions, A_1 and A_5, from Table I as

$$A_1(\bar{r}) = \left(1-\frac{2}{\bar{r}}\right)^{1/2}\left(1-\frac{2\bar{r}^2}{(\bar{r}^2+\bar{q}_{\rm m}^2)^{3/2}}\right)^{-1/2}, \tag{B3}$$

$$A_5(\bar{r}) = \left(1-\frac{2}{\bar{r}}\right)^{-1}\left(1-\frac{2\bar{r}^2}{(\bar{r}^2+\bar{q}_{\rm m}^2)^{3/2}}\right), \tag{B4}$$

where in the above we have introduced $\bar{r} = r/M$ for brevity. Also, the parameter $\bar{q}_{\rm m}$ corresponds to the parameter g/M of Ref. [77]. We obtain now the CY coefficients α_{i0} up to fifth order for this spacetime as

$$\alpha_{10}=1,\ \ \alpha_{13}=-\frac{3\bar{q}_{\rm m}^2}{2},\ \ \alpha_{14}=-3\bar{q}_{\rm m}^2,\ \ \alpha_{15}=-6\bar{q}_{\rm m}^2+\frac{15\bar{q}_{\rm m}^4}{8},$$
$$\alpha_{50}=1,\ \ \alpha_{53}=3\bar{q}_{\rm m}^2,\ \ \alpha_{54}=6\bar{q}_{\rm m}^2,\ \ \alpha_{55}=12\bar{q}_{\rm m}^2-\frac{15\bar{q}_{\rm m}^4}{8}, \tag{B5}$$

which can be verified to match the expressions in Table 1 of Ref. [77]. From the form of the functions in Eq. (B3), it is clear that for appreciable specific magnetic charges $0 \lesssim \bar{q}_{\rm m}$, close to the horizon, which lies between $1.23 \lesssim \bar{r}_{\rm H} \lesssim 1.99$, arbitrarily high-order coefficients might become important in this parametrization scheme. We demonstrate this by showing in Fig. 2 how the impact parameter of a photon on the unstable circular geodesic in this spacetime, which is a near-horizon observable, is approximated within both the CY parametrization scheme and in our scheme.

TABLE IV. Here we show the relative error in approximating the first and second derivatives of the metric functions for all of the BH and non-BH spacetimes considered here.

		Maximum relative error			
Spacetime	Physical charge	dN/dx	d^2N/dx^2	dB/dx	d^2B/dx^2
RN	$\bar{q}=0.5$	0	0	0	0
	$\bar{q}=0.9$	0	0	0	0
E-ae 2	[0.1, 0.1]	0	0	0	0
$[c_{13}, c_{14}]$	[0.1, 0.9]	0	0	0	0
	[0.9, 1.7]	0	0	0	0
E-ae 1	$c_{13}=0.5$	0	0	0	0
	$c_{13}=0.9$	0	0	0	0
Bardeen	$\bar{q}_{\rm m}=0.25$	0	3.04 [−9]	0	0
	$\bar{q}_{\rm m}=0.75$	2.10 [−5]	1.09 [−3]	0	0
Hayward	$\bar{l}=0.25$	8.25 [−7]	5.35 [−6]	0	0
	$\bar{l}=0.75$	3.39 [−4]	5.43 [−3]	0	0
Bronnikov	$\bar{q}_{\rm m}=0.5$	0	0	0	0
	$\bar{q}_{\rm m}=1.05$	2.74 [−7]	7.17 [−6]	0	0
EEH	[1, 0.05]	1.96 [−5]	3.93 [−2]	0	0
$[\bar{q}_{\rm m}, \bar{\alpha}]$	[1, 1]	1.31 [−4]	4.75 [−2]	0	0
Frolov	[0.5, 0.25]	1.60 [−6]	1.22 [−5]	0	0
$[\bar{q}, \bar{l}]$	[0.5, 0.6]	2.16 [−4]	3.76 [−3]	0	0
	[0.9, 0.25]	3.59 [−5]	9.83 [−4]	0	0
KS	$\bar{a}=1$	4.60 [−7]	2.93 [−6]	0	0
	$\bar{a}=10$	3.80 [−2]	6.93 [−2]	0	0
CFM A	$\beta=-0.9$	0	0	2.03 [−3]	2.01 [−2]
	$\beta=0.9$	0	0	2.65 [−6]	1.74 [−5]
CFM B	$\beta=1.1$	0	0	4.46 [−5]	7.7 [−5]
	$\beta=1.2$	0	0	7.26 [−3]	4.04 [−3]
Mod. Hayward	$\bar{l}=0.25$	8.25 [−7]	5.35 [−6]	9.96 [−2]	1.94 [−1]
	$\bar{l}=0.75$	3.39 [−4]	5.43 [−3]	9.20 [−2]	1.69 [−1]
EMd	$\bar{q}=0.7$	0	0	1.43 [−6]	1.32 [−6]
	$\bar{q}=1.4$	1.74 [−2]	4.29 [−2]	3.09 [−2]	6.58 [−2]
MBS A	⋯	4.79 [−2]	1.92 [−2]	8.06 [−2]	3.68 [−2]
MBS B	⋯	1.88 [−1]	2.94 [−1]	2.22 [−1]	5.08 [−1]
JNW	$\nu=0.1$	1.45 [−2]	3.55 [−2]	4.04 [−1]	2.60 [−2]
	$\nu=0.5$	4.31 [−3]	2.51 [−1]	1.02 [−2]	2.91 [−3]
	$\nu=0.9$	1.61 [−3]	1.31 [−2]	5.27 [−2]	2.63 [−2]

TABLE V. Here we demonstrate the rapidity of convergence of the parametrization scheme used here by estimating the relative error in obtaining the unstable circular null geodesic impact factor $\xi_{\rm ps}$ and the ISCO frequency $\Omega_{\rm ISCO}$ at orders two and four in the current parametrization scheme. We have omitted below those spacetimes for which the only relevant metric function N for these observables is already exactly recovered at a lower order.

		Maximum relative error			
		$\xi_{\rm ps}$		$\Omega_{\rm ISCO}$	
Spacetime	Physical charge	$a_3=0$	$a_5=0$	$a_3=0$	$a_5=0$
Bardeen	$\bar{q}_{\rm m}=0.25$	3.71 [−6]	0	2.00 [−6]	1.49 [−9]
	$\bar{q}_{\rm m}=0.75$	3.10 [−3]	7.35 [−6]	6.74 [−3]	2.21 [−5]
Hayward	$\bar{l}=0.25$	1.78 [−5]	1.20 [−7]	3.28 [−6]	2.56 [−6]
	$\bar{l}=0.75$	5.44 [−2]	1.29 [−4]	1.02 [−1]	2.26 [−4]
Bronnikov	$\bar{q}_{\rm m}=0.5$	×	×	0	0
	$\bar{q}_{\rm m}=1.05$	×	×	1.22 [−3]	2.95 [−8]
EEH	[1, 0.05]	×	×	8.31 [−4]	4.44 [−7]
$[\bar{q}_{\rm m},\bar{\alpha}]$	[1, 1]	×	×	4.68 [−3]	2.22 [−4]
Frolov	[0.5, 0.25]	4.18 [−5]	2.66 [−7]	2.09 [−5]	4.37 [−6]
$[\bar{q},\bar{l}]$	[0.5, 0.6]	1.17 [−1]	7.87 [−5]	5.66 [−1]	1.59 [−4]
	[0.9, 0.25]	1.10 [−2]	1.47 [−5]	2.12 [−1]	3.80 [−6]
KS	$\bar{a}=1$	9.31 [−6]	6.66 [−8]	1.39 [−6]	1.45 [−6]
	$\bar{a}=10$	2.78 [−2]	8.62 [−3]	1.11 [−1]	4.34 [−2]
Mod. Hayward	$\bar{l}=0.25$	5.44 [−2]	1.29 [−4]	1.02 [−1]	2.26 [−4]
	$\bar{l}=0.75$	1.78 [−5]	1.20 [−7]	3.28 [−6]	2.56 [−6]
EMd	$\bar{q}=0.7$	4.43 [−7]	0	3.97 [−7]	0
	$\bar{q}=1.4$	7.62 [−1]	7.22 [−3]	2.93 [−1]	6.84 [−3]
MBS A	⋯	×	×	×	×
MBS B	⋯	×	×	×	×
JNW	$\nu=0.1$	×	×	×	×
	$\nu=0.5$	×	×	3.54 [−3]	7.81 [−3]
	$\nu=0.9$	2.86 [−3]	6.95 [−4]	7.85 [−3]	1.11 [−3]

APPENDIX C: GOODNESS OF APPROXIMATION AND CONVERGENCE TESTS

The fourth-order approximations of the metric functions for the various spacetimes under consideration here are smooth throughout the range of the conformal coordinate $0 \leq x < 1$. To demonstrate the accuracy in obtaining the metric function up to two derivatives, we report the relative errors in approximating them in Table IV, which are typically appreciably low.

We also demonstrate the rapidity of the order-on-order convergence of our parametrization scheme by estimating the relative error in obtaining the unstable circular null geodesic impact factor $\xi_{\rm ps}$ and ISCO frequency $\Omega_{\rm ISCO}$ at the second and fourth orders in Padé expansion. This is reported in Table V. We gain about two orders of accuracy by going two orders higher in the Padé expansion.

[1] K. S. Thorne and C. M. Will, Astrophys. J. **163**, 595 (1971).
[2] R. H. Dicke, Gen. Relativ. Gravit. **51**, 57 (2019) [republication].
[3] C. M. Will, Living Rev. Relativity **17**, 4 (2014).
[4] C. W. Misner, K. S. Thorne, and J. A. Wheeler, *Gravitation* (Freeman, San Francisco, 1973).
[5] C. M. Will, Astrophys. J. **163**, 611 (1971).
[6] C. M. Will, Astrophys. J. **169**, 125 (1971).
[7] A. Einstein, Ann. Phys. (N.Y.) **354**, 769 (1916).
[8] T. E. Collett, L. J. Oldham, R. J. Smith, M. W. Auger, K. B. Westfall, D. Bacon, R. C. Nichol, K. L. Masters, K. Koyama, and R. van den Bosch, Science **360**, 1342 (2018).
[9] J. H. Taylor and J. M. Weisberg, Astrophys. J. **253**, 908 (1982).

[10] K. Akiyama *et al.*, Astrophys. J. **875**, L1 (2019).
[11] K. Akiyama *et al.*, Astrophys. J. **875**, L2 (2019).
[12] K. Akiyama *et al.*, Astrophys. J. **875**, L3 (2019).
[13] K. Akiyama *et al.*, Astrophys. J. **875**, L4 (2019).
[14] K. Akiyama *et al.*, Astrophys. J. **875**, L5 (2019).
[15] K. Akiyama *et al.*, Astrophys. J. **875**, L6 (2019), https://iopscience.iop.org/journal/2041-8205/page/Focus_on_EHT.
[16] B. P. Abbott *et al.*, Phys. Rev. Lett. **116**, 061102 (2016).
[17] B. P. Abbott *et al.*, Astrophys. J. Lett. **818**, L22 (2016).
[18] R. Abuter *et al.*, Astron. Astrophys. **615**, L15 (2018).
[19] R. Abuter *et al.*, Astron. Astrophys. **636**, L5 (2020).
[20] R. Shaikh, P. Kocherlakota, R. Narayan, and P. S. Joshi, Mon. Not. R. Astron. Soc. **482**, 52 (2019).
[21] H. Olivares, Z. Younsi, C. M. Fromm, M. De Laurentis, O. Porth, Y. Mizuno, H. Falcke, M. Kramer, and L. Rezzolla, Mon. Not. R. Astron. Soc. **497**, 521 (2020).
[22] G. D. Birkhoff, *Relativity and Modern Physics* (Harvard University Press, Cambridge, 1923).
[23] M. Sasaki and T. Nakamura, Gen. Relativ. Gravit. **22**, 1351 (1990).
[24] M. Dafermos and I. Rodnianski, arXiv:1010.5132.
[25] J. Lucietti and H. S. Reall, Phys. Rev. D **86**, 104030 (2012).
[26] K. Düztaş and I. Semiz, Phys. Rev. D **88**, 064043 (2013).
[27] M. Dafermos, I. Rodnianski, and Y. Shlapentokh-Rothman, arXiv:1402.7034.
[28] K. Düztaş, Classical Quantum Gravity **32**, 075003 (2015).
[29] Y. Shlapentokh-Rothman, Ann. Henri Poincaré **16**, 289 (2015).
[30] J. Natário, L. Queimada, and R. Vicente, Classical Quantum Gravity **33**, 175002 (2016).
[31] M. Richartz, Phys. Rev. D **93**, 064062 (2016).
[32] M. Sasaki and T. Nakamura, Prog. Theor. Phys. **67**, 1788 (1982).
[33] J. C. Miller and S. Motta, Classical Quantum Gravity **6**, 185 (1989).
[34] H.-J. Yo, T. W. Baumgarte, and S. L. Shapiro, Phys. Rev. D **66**, 084026 (2002).
[35] L. Baiotti, I. Hawke, P. J. Montero, F. Löffler, L. Rezzolla, N. Stergioulas, J. A. Font, and E. Seidel, Phys. Rev. D **71**, 024035 (2005).
[36] A. Nathanail, E. R. Most, and L. Rezzolla, Mon. Not. R. Aston. Soc. **469**, L31 (2017).
[37] D. Christodoulou, Commun. Math. Phys. **93**, 171 (1984).
[38] D. Christodoulou, Commun. Math. Phys. **105**, 337 (1986).
[39] S. L. Shapiro and S. A. Teukolsky, Phil. Trans. R. Soc. A **340**, 365 (1992), https://www.jstor.org/stable/54004.
[40] M. W. Choptuik, Phys. Rev. Lett. **70**, 9 (1993).
[41] D. Christodoulou, Ann. Math. **140**, 607 (1994).
[42] D. Christodoulou, Ann. Math. **149**, 183 (1999).
[43] T. Harada, H. Iguchi, and K.-I. Nakao, Prog. Theor. Phys. **107**, 449 (2002).
[44] T. Crisford and J. E. Santos, Phys. Rev. Lett. **118**, 181101 (2017).
[45] R. Penrose, Phys. Rev. Lett. **14**, 57 (1965).
[46] R. Penrose, Gen. Relativ. Gravit. **34**, 1141 (2002) [republication].
[47] R. Penrose, in *General Relativity, an Einstein Centenary Survey*, edited by S. Hawking and W. Israel (Cambridge University Press, Cambridge, 1979), p. 581, https://ui.adsabs.harvard.edu/abs/2010grae.book.....H/abstract.
[48] S. W. Hawking and G. F. R. Ellis, *The Large Scale Structure of Space Time* (Cambridge University Press, Cambridge, England, 1973).
[49] G. Lemaître and M. A. H. MacCallum, Gen. Relativ. Gravit. **29**, 641 (1997); R. C. Tolman, Proc. Natl. Acad. Sci. U.S.A. **20**, 12 (1934); H. Bondi, Mon. Not. R. Astron. Soc. **107**, 410 (1947).
[50] D. M. Eardley and L. Smarr, Phys. Rev. D **19**, 2239 (1979).
[51] L. Rezzolla and A. Zhidenko, Phys. Rev. D **90**, 084009 (2014).
[52] T. Damour, Classical Quantum Gravity **13**, A33 (1996).
[53] T. Damour, Classical Quantum Gravity **29**, 184001 (2012).
[54] C. Eling, T. Jacobson, and D. Mattingly, arXiv:gr-qc/0410001.
[55] E. Ayon-Beato and A. Garcia, Phys. Lett. B **464**, 25 (1999).
[56] K. Schwarzschild, Sitzungsberichte der Königlich Preussischen Akademie der Wissenschaften **7**, 189 (1916), https://ui.adsabs.harvard.edu/abs/1916SPAW.....189S/abstract.
[57] H. Reissner, Ann. Phys. (N.Y.) **355**, 106 (1916); G. Nordström, in *Koninkl. Ned Akad. Wetenschap. Proceedings, 1918* (1918), p. 1238, https://ui.adsabs.harvard.edu/abs/1918KNAB...20.1238N/abstract.
[58] J. M. Bardeen, in *Proceedings of the Int. Conf. GR5, 1393* (Tbilisi University Press, U.S.S.R, 1968), p. 174, http://www.isgrg.org/pastconfs.php.
[59] S. A. Hayward, Phys. Rev. Lett. **96**, 031103 (2006).
[60] A. Held, R. Gold, and A. Eichhorn, J. Cosmol. Astropart. Phys. 6 (2019) 029.
[61] V. P. Frolov, Phys. Rev. D **94**, 104056 (2016).
[62] P. Berglund, J. Bhattacharyya, and D. Mattingly, Phys. Rev. D **85**, 124019 (2012).
[63] D. I. Kazakov and S. N. Solodhukin, Nucl. Phys. **B429**, 153 (1994).
[64] R. Casadio, A. Fabbri, and L. Mazzacurati, Phys. Rev. D **65**, 084040 (2002).
[65] A. García, D. Galtsov, and O. Kechkin, Phys. Rev. Lett. **74**, 1276 (1995).
[66] G. W. Gibbons and K.-I. Maeda, Nucl. Phys. **B298**, 741 (1988).
[67] D. Garfinkle, G. T. Horowitz, and A. Strominger, Phys. Rev. D **43**, 3140 (1991); **45**, 3888(E) (1992).
[68] K. A. Bronnikov, Phys. Rev. D **63**, 044005 (2001).
[69] H. Yajima and T. Tamaki, Phys. Rev. D **63**, 064007 (2001).
[70] A. I. Janis, E. T. Newman, and J. Winicour, Phys. Rev. Lett. **20**, 878 (1968).
[71] R. A. Konoplya and A. Zhidenko, Phys. Rev. D **101**, 124004 (2020).
[72] R. Konoplya, L. Rezzolla, and A. Zhidenko, Phys. Rev. D **93**, 064015 (2016).
[73] Z. Younsi, A. Zhidenko, L. Rezzolla, R. Konoplya, and Y. Mizuno, Phys. Rev. D **94**, 084025 (2016).
[74] R. Arnowitt, S. Deser, and C. W. Misner, Gen. Relativ. Gravit. **40**, 1997 (2008) [republished].

[75] G. A. Baker, Jr. and P. R. Graves-Morris, *Padé Approximants* (Cambridge University Press, Cambridge, England, 1996).
[76] C. M. Bender and S. A. Orszag, *Advanced Mathematical Methods for Scientists and Engineers I* (Springer-Verlag, New York, 1999).
[77] Z. Carson and K. Yagi, Phys. Rev. D **101**, 084030 (2020).
[78] J. Magueigo, Rep. Prog. Phys. **66**, 2025 (2003).
[79] T. Jacobson, arXiv:0711.3822.
[80] T. Jacobson, *Proc. Sci.*, QG-PH2007 (2007) 020 [arXiv:0801.1547].
[81] K. Hioki and K.-I. Maeda, Phys. Rev. D **80**, 024042 (2009).
[82] P. Kocherlakota, P. S. Joshi, S. Bhattacharyya, C. Chakraborty, A. Ray, and S. Biswas, Mon. Not. R. Astron. Soc. **490**, 3262 (2019).
[83] M. De Laurentis, Z. Younsi, O. Porth, Y. Mizuno, and L. Rezzolla, Phys. Rev. D **97**, 104024 (2018).
[84] S. Weinberg, in *Gravitation and Cosmology: Principles and Applications of the General Theory of Relativity* (Wiley, New York, 1972), pp. 8.4, 8.5.
[85] A. G. Suvorov, Classical Quantum Gravity **37**, 185001 (2020).
[86] Z. Bern and A. G. Morgan, Phys. Rev. D **49**, 6155 (1994).
[87] P. Stehle and P. G. DeBaryshe, Phys. Rev. **152**, 1135 (1966).
[88] R. R. Cuzinatto, C. A. M. de Melo, K. C. de Vasconcelos, L. G. Medeiros, and P. J. Pompeia, Astrophys. Space Sci. **359**, 59 (2015).
[89] M. Novello, V. A. De Lorenci, J. M. Salim, and R. Klippert, Phys. Rev. D **61**, 045001 (2000).
[90] M. Novello, S. E. P. Bergliafa, and J. M. Salim, Classical Quantum Gravity **17**, 3821 (2000).
[91] E. Ayon-Beato and A. Garcia, Phys. Lett. B **493**, 149 (2000).
[92] A. D. Sakharov, Sov. Phys. JETP **22**, 241 (1966), http://www.jetp.ac.ru/cgi-bin/e/index/e/22/1/p241?a=list.
[93] E. B. Gliner, Sov. Phys. JETP **22**, 378 (1966), http://www.jetp.ac.ru/cgi-bin/e/index/e/22/2/p378?a=list.
[94] M. A. Markov, JETP Lett. **36**, 265 (1982), http://www.jetpletters.ac.ru/ps/1334/article_20160.shtml.
[95] V. P. Frolov, M. A. Markov, and V. F. Mukhanov, Phys. Rev. D **41**, 383 (1990).
[96] V. Mukhanov and R. Brandenberger, Phys. Rev. Lett. **68**, 1969 (1992).
[97] R. Brandenberger, V. Mukhanov, and A. Sornborger, Phys. Rev. D **48**, 1629 (1993).
[98] D. J. Kaup, Phys. Rev. **172**, 1331 (1968).
[99] K. S. Virbhadra, Int. J. Mod. Phys. A **12**, 4831 (1997).
[100] K. S. Virbhadra, S. Jhingan, and P. S. Joshi, Int. J. Mod. Phys. D **06**, 357 (1997).
[101] M. Patil and P. S. Joshi, Phys. Rev. D **85**, 104014 (2012).
[102] A. N. Chowdhury, M. Patil, D. Malafarina, and P. S. Joshi, Phys. Rev. D **85**, 104031 (2012).
[103] K. D. Kokkotas, R. A. Konoplya, and A. Zhidenko, Phys. Rev. D **96**, 064004 (2017).
[104] K. D. Kokkotas, R. A. Konoplya, and A. Zhidenko, Phys. Rev. D **96**, 064007 (2017).
[105] R. A. Konoplya and A. Zhidenko, Phys. Rev. D **100**, 044015 (2019).
[106] R. A. Konoplya, T. D. Pappas, and Z. Stuchlík, arXiv:2007.14860.
[107] P. O. Mazur and E. Mottola, arXiv:gr-qc/0109035.
[108] O. Porth, H. Olivares, Y. Mizuno, Z. Younsi, L. Rezzolla, M. Moscibrodzka, H. Falcke, and M. Kramer, Comput. Astrophys. **4**, 1 (2017).
[109] H. Olivares, O. Porth, J. Davelaar, E. R. Most, C. M. Fromm, Y. Mizuno, Z. Younsi, and L. Rezzolla, Astron. Astrophys. **629**, A61 (2019).
[110] Y. Mizuno, Z. Younsi, C. M. Fromm, O. Porth, M. De Laurentis, H. Olivares, H. Falcke, M. Kramer, and L. Rezzolla, Nat. Astron. **2**, 585 (2018).
[111] S. H. Völkel and K. D. Kokkotas, Phys. Rev. D **100**, 044026 (2019).
[112] S. H. Völkel and E. Barausse, arXiv:2007.02986.